Temperature and Concentration Dependence of the Ionic Transport Properties of Lithium-Ion Battery Electrolytes

Temperature and Concentration Dependence of the Ionic Transport Properties of Lithium-Ion Battery Electrolytes

Johannes Landesfeind [z] **and Hubert A. Gasteiger***

Chair of Technical Electrochemistry, Department of Chemistry and Catalysis Research Center, Technical University of Munich, Munich, Germany

Lithium-ion battery performance at low temperatures or fast charge/discharge rates is determined by the intrinsic electrolyte transport and the thermodynamic properties of the commonly used binary electrolytes. For the development of future electrolyte solutions, a quantification of the ionic conductivity, the binary diffusion coefficient, the transference number, and the thermodynamic factor over a large concentration and temperature range is mandatory. In this study, we apply previously discussed and established methods for the determination of ionic conductivities and binary diffusion coefficients to two commonly used electrolyte systems (EC:DMC (1:1 w:w) and EC:EMC (3:7 w:w)) as well as to one EC-free electrolyte (EMC:FEC (19:1 w:w)). To quantify transference numbers and thermodynamic factors, we introduce a novel analysis scheme, so that we are ultimately able to report temperature (−10°C–+50°C) and concentration (0.1 M–3.0 M) dependent values as well as approximate relationships for transport and thermodynamic properties required for numerical battery models. Comparison with scarcely available literature data highlights that the hitherto reported concentration and temperature dependencies do not reflect the complexity of ionic transport properties, which will likely lead to imprecise predictions of, e.g., a lithium-ion battery's power limitations or the onset of lithium plating.
 [DOI: 10.1149/2.0571912jes]

Manuscript submitted February 27, 2019; revised manuscript received July 1, 2019. Published September 13, 2019.

During the operation of lithium-ion batteries, ionic concentration gradients evolve in the liquid electrolyte, especially when the cell is cycled at high charge/discharge currents or at low temperatures. For a profound understanding of the performance vs. charge/discharge rate and of detrimental side effects, such as lithium plating during charging at high rate and/or low temperature, the ionic transport properties of the electrolyte have to be known precisely. While the transport path length is largely determined by the tortuosity of the porous media,[1–3] the intrinsic ionic transport properties according to the widely applied Newman model[4] are the ionic conductivity (κ), the binary diffusion coefficient ($D_{\pm}$),[5] the cationic transference number (t_+),[6] and the thermodynamic factor (TDF $\equiv 1+\mathrm{dln}(f_{\pm})/\mathrm{dln}(c)$; with $f_{\pm}$ being the mean molar activity coefficient).[7] The ionic conductivity is the proportionality factor in the relation between the ohmic potential drop in the electrolyte and the total current in the absence of diffusion and convection, while the binary diffusion coefficient describes an averaged diffusivity of the charge carrying ions in the electrolyte, i.e., the proportionality coefficient between flux and concentration gradient. Upon an electrochemical reaction at the electrodes, an electric field will be established which is the driving force for the migration of ions. The fraction of this migration current that is carried by the cations or anions is called cationic or anionic transference number. The mean molar activity coefficient is the averaged form of the molar activity coefficients for anion and cation; the derivative of the logarithm of the mean molar activity coefficient with the logarithm of the salt concentration is an essential part of the so-called thermodynamic factor. Molar activity coefficients themselves relate the reactivity of an ion in an electrolyte to its reactivity at infinite dilution.

Despite their importance, concentration and more importantly also temperature dependent studies of ionic transport in typical lithium-ion battery electrolyte solutions are scarce. Apart from the well-known groundwork by Valøen and Reimers, only few experimental studies are known to the authors which provide a comprehensive set of transport properties in non-aqueous lithium-ion electrolytes over a reasonable concentration and temperature range.[8–11] The measurement scheme conducted by Bruce and Vincent for polymer electrolytes is based on the dilute solution theory, which,[12,13] e.g., neglects activity coefficients and is not applicable for concentrated electrolyte solutions as discussed previously.[6] As the experimental quantification of electrolyte transport properties is cumbersome, recent studies report theoretical predictions of electrolyte transport parameters for mixed salt systems in nonaqueous solvent mixtures for lithium- and sodium-ion batteries. Thus, the advanced electrolyte model (AEM) by Gering includes solvent-ion and ion-ion effects, the change in viscosity, counter-ion transport, ionic hoping, and ionic random motion effects.[14] It is claimed that osmotic coefficients and activity coefficients for multi-solvent and mixed-salt aqueous solutions can be predicted with the molecular AEM approach with less than 1% absolute average deviation for some specific electrolytes.[15] Recently, the AEM was critically evaluated for a large range of lithium-ion battery electrolyte compositions, and generally good agreement between experimentally determined viscosities and conductivities and the predictions from the AEM were found.[16] Beside the comparison of the AEM with experimentally determined electrolyte conductivities by Valøen and Reimers in Ref. 14, to the best of our knowledge there are no publications yet which compare the AEM predictions for diffusion coefficient, transference number, or activity coefficients of lithium ion battery electrolytes with experimentally determined values. Thus, a validation of these transport property predictions by the AEM remains to be shown for lithium-ion battery electrolyte solutions, which is difficult due to the lack of comprehensive sets of experimental data. In a recent study by Farkhondeh et al.,[17] an optimization approach for pulse experiments in a four-electrode cell setup is presented, and the transport parameters are reported for two electrolytes with 1 M $LiPF_6$ at 25°C. Even though this method may be applied to other salt concentrations and temperatures in order to obtain more comprehensive data sets, it requires experience in optimization routines and the simulation of battery cells which may prevent its wide application by electrolyte developers.

In this work, we present simple experimental techniques that may be applied by the majority of laboratories working on lithium-ion batteries and guide through the straightforward analysis which does not require extensive model analysis, but may be done using simple spreadsheet calculations. Building on our previous efforts to analyze various determination methods for the quantification of binary diffusion coefficients[5] and transference numbers,[6] we analyze two typical battery electrolytes and one novel ethylene carbonate free electrolyte which was proposed in the literature[18] (see Experimental section for electrolyte compositions). Unfortunately, a recently conducted careful analysis of our previously introduced direct determination method for the thermodynamic factor (TDF) of binary lithium-ion battery electrolytes based on cyclic voltammograms of the ferrocene/ferrocenium

*Electrochemical Society Fellow.
[z]E-mail: j.landesfeind@tum.de

couple[7] identified that one of the underlying assumptions was invalid, discussed in more detail for the interested reader in the corresponding erratum.[19] Thus, quantification of the transference number and the thermodynamic factor in the present study is not based on these ferrocene/ferrocenium based experiments, but we introduce a novel modification of the analytical method based on concentration cell potentials and galvanostatic pulse experiments in symmetric lithium cells. The here proposed approach requires three cell setups to quantify the electrolyte transport properties: i) a conductivity cell allowing for electrochemical impedance measurements; ii) a pouch cell based concentration cell to determine the open circuit voltage between two lithium electrodes immersed in electrolytes with different salt concentrations, and, iii) a coin cell with two lithium electrodes to record the short-term and the long-term potential transients after a galvanostatic pulse. The finally obtained values for the ionic transport properties span the concentration range from 0.1 M to 3.0 M and were obtained at temperatures from −10°C to +50°C in 10°C steps for the three electrolytes specified above. We will critically compare our results with suitable publications from the literature and will highlight the often assumed oversimplified concentration and temperature dependencies.

In the following, we first introduce the experimental procedures and setups used for the determination of transport properties in this work. Our previously presented methods[5,6] for the parameter determination are recapitulated briefly in the Theory section, and we introduce a simple scheme, useable as a manual for the measurement of ionic transport properties in battery electrolytes. Subsequently, exemplary datasets will be used to illustrate the data processing and analysis in great detail and to help to judge the errors in the final results. The Results section summarizes the found temperature and concentration dependent values for the four binary electrolyte properties (i.e., κ, $D_{\pm}$, t_+, and TDF) and provides fitting parameters and their errors to empirically and semi-empirically chosen temperature and concentration dependent functional approximations. To account for the complexity of temperature and concentration dependent transference numbers and thermodynamic factors, we additionally present individual analyses of those parameters on a per temperature basis for the benefit of the reader. The Supporting Information gives background analyses and measurements not required to follow the main study and is referred to at the appropriate sections in the main article.

Experimental

Electrolyte and cell material specifications.—Mixtures of ethylene carbonate (EC, BASF, battery grade/Sigma Aldrich, anhydrous, 99%), ethyl-methylene carbonate (EMC, BASF, battery grade), dimethyl carbonate (DMC, Sigma Aldrich, anhydrous, 99%) and fluoroethylene carbonate (FEC, BASF, battery grade) were used as solvents for self-prepared electrolytes containing lithium hexafluorophosphate ($LiPF_6$, BASF, battery grade/Sigma Aldrich, 99.99%) salt, mixed in an argon filled and temperature controlled glove box (MBraun, 25°C ± 1°C, water content < 0.1 ppm, Ar 5.0, Westfalen, 99.999% Vol). $LiPF_6$ concentrations of 0.1, 0.5, 1.0, 1.5, 2.0 and 3.0 M will be referred to as base concentrations. Additionally 0.01 M electrolytes were prepared for the use in concentration cells. Unless stated otherwise, throughout this manuscript we use M to denominate volumetric concentrations (in moles/L). For the interested reader, we provide density measurements for the electrolytes used in this study, covering the used temperature and concentration range (see Supporting Information (SI), Figure S1; fitting parameters to a linear concentration and temperature dependent function (Eq. S1) are given in Table S1 in the SI). Metallic lithium (Rockwood Lithium, 75 µm or 450 µm thickness, high purity) was used as counter electrode (CE) and working electrode (WE) in concentration cells and coin cells.

Due to trace hydrofluoric acid (HF) concentrations in the electrolytes, the glass-fiber separators used previously for short measurements at room temperature[6] could not be used in this study, as ongoing gas evolution during the much longer measurements, particularly at higher temperatures, will lead to an expansion of the pouch cell in concentration cell measurements. Therefore, porous polyethylene films (PE, Nitto, Sunmap LC, 500 µm thickness, 30% porosity) were used as a separator in this study. To ensure good wettability of the PE separator, especially with the EC:DMC (1:1 w:w) electrolyte at high salt concentrations, all Nitto separators were nitrogen plasma treated for five minutes (PlasmaFlecto 10, plasma technology, 0.3 mbar, 300 W) and assembled within the cells within one week.

All coin and pouch cell parts were dried overnight in a vacuum drying oven at 70°C before bringing them into the glove box. Measurements were conducted outside the glove box using a Biologic VMP3 potentiostat/galvanostat or a Biologic SP-300 potentiostat/galvanostat.

Conductivity cell design and measurements.—The ionic conductivity of all electrolytes at their base concentrations was determined in a commercially available Pt microelectrode setup (rhd Instruments, TSC 1600 closed, Germany), consisting of a Pt beaker and a Pt microelectrode (see Figure 1, left panel), temperature-controlled using an external Peltier element and controller unit (not shown in Figure 1). A small sample volume (1 mL), which allows for a fast temperature equilibration, was filled into the cleaned cell inside the glove box, and impedance measurements were done outside the glove box between both Pt electrodes in a frequency range from 85 kHz to 1 kHz and with an excitation amplitude of 100 mV. Prior to the electrolyte measurements, the cell constant k_C was determined using 0.001, 0.01 and 0.1 M KCl calibration solutions (Sigma Aldrich, conductance standard A, B and C) at 25°C, yielding $k_C = 20.0 \pm 0.2$ 1/cm). Cell impedances with lithium-ion electrolytes were measured first at +50°C after a 10 min equilibration time; subsequently the cell temperature was decreased in 10°C steps down to −10°C and 5 min equilibration times were used after the set-point temperatures were reached. Conductivity measurements were only done once for each concentration and temperature due to the very good agreement with values from the manufacturer (see Figure S2 in the SI) and the small error of the measurement (see 1% error for the cell constant calibration).

Concentration cell design and measurements.—Pouch cells for the temperature dependent measurement of concentration potentials (see Figure 1) were prepared inside the glove box. The cell dimensions of ∼5 cm (width) × ∼13 cm (length) were chosen to accommodate a 1 cm wide, 500 µm thick, and 10 cm long Nitto separator, positioned on top of the lithium electrodes (450 µm thick) which were attached to Ni tabs (MTI cooperation) equipped with a sealing tape. Two electrolyte solutions of differential concentrations (in this study pairs of adjacent base concentrations including the 0.01 M electrolyte, i.e., 0.01–0.1 M, 0.1–0.5 M, etc.) were carefully added at the left and right ends of the separator. Care was taken that the electrolytes are soaked up by the porous separator and do not spill in the cell volume. The total electrolyte amount was calculated from the theoretically available pore space in the separator (150 µl) and was sufficient to see the electrolyte wetted regions to contact in the middle of the separator before the cell was sealed at 50 mbar using a vacuum sealing device (C 70, multivac, Germany) inside the glove box (the cell was first sealed at the sides and the top to fix the tabs). The 10 cm length of the separator assured that no complete mixing of electrolyte would occur within the measurement time of several hours, compared to the estimated diffusion time constant of ∼36 days (from $(5\ \text{cm})^2/(8 \cdot 10^{-6}\ \text{cm}^2/\text{s})$, using the highest binary diffusion coefficient obtained in our measurements (see Figure 8)).

Multiple pouch concentration cells (up to eight) were stacked between copper plates of equal size each (∼5 cm × 13 cm × 0.5 cm) and the entire stack was immersed into an ethylene glycol / water bath (∼50:50 by weight) of a refrigerated circulator (Julabo FP 50, HL, Germany), with the Ni tabs facing upwards and positioned ∼1 cm above the liquid level. The setup ensures a fast temperature equilibration and a very homogeneous temperature distribution across the pouch concentration cells, a requirement which could not be met reproducibly when using a temperature convection chamber. Open circuit voltages (U_{CC}) of at least two cells for each temperature and concentration were measured for three minutes after reaching the set-point temperature

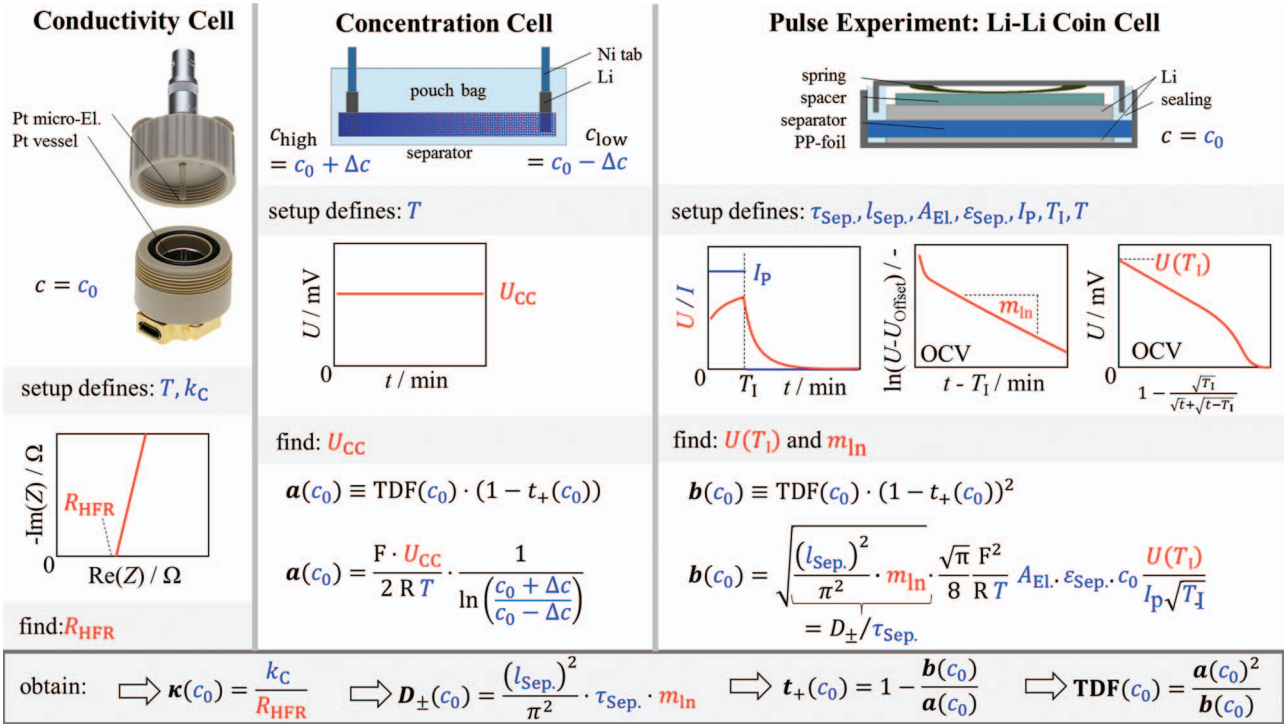

Figure 1. Scheme to determine the transport and thermodynamic parameters with measurements around a base salt concentration c_0. Slight modifications to this scheme are discussed in the main text (see section Data Analysis) due to the necessity to increase the concentration differences of the concentration cells to observe temperature effects. Left panel: The ionic conductivity (κ) is determined with a temperature-controlled conductivity cell (rhd Instruments) with a cell constant k_C, based on the resistance (R_{HFR}) determined by impedance spectroscopy. Middle panel: Concentration cell potentials (U_{CC}) are obtained with a pouch cell setup, using two identical lithium metal electrodes exposed to electrolytes with different salt concentrations ($c_0+\Delta c$ and c_0-Δc); this allows to quantify the factor *a*. Right panel: The open circuit voltage (OCV) relaxation after a galvanostatic pulse applied to a coin cell with two identical lithium metal electrodes allows to determine the binary diffusion coefficient ($D_\pm$; solely from the long-term OCV relaxation) and the factor *b* (from the potential just after the end of the current pulse ($U(T_I)$ and $D_\pm$). Lower horizontal panel: From the measurement data (marked in red) and the used parameters/settings (marked in blue), the temperature and concentration dependence of the four electrolyte parameters (κ, $D_\pm$, t_+, and TDF) can be quantified. Input parameters are the separator tortuosity ($\tau_{Sep.}$), the thickness of the separator ($l_{Sep.}$), the area of the electrode ($A_{El.}$), the void volume fraction of the separator ($\varepsilon_{Sep.}$), the pulse current value (I_p), the duration of the current pulse (T_I), the temperature (*T*) as well as the the Faraday constant (F), and the gas constant (R).

(from −10°C to +50°C in 10°C steps, starting at low temperatures to limit diffusion effects) with a potentiostat (Biologic, SP300), and the mean value during the full measurement period was taken as the final U_{CC} value.

Coin cells.—Pulse experiments in symmetrical Li-Li cells were conducted in coin cells (MTI cooperation, compare Figure 1) assembled inside a glove box. A 17 mm Li electrode (75 µm thickness) and a 1 mm polypropylene foil ring (17 mm inner diameter, 19 mm outer diameter, ∼80 µm thickness) were centrally positioned into the larger can of the coin cell before putting a 19 mm separator disk (plasma treated 500 µm thick Nitto separator) on top. The cell assembly was finished by first adding the coin cell sealing ring, slowly adding the electrolyte (60 µL, corresponding to ∼150% of the separator pore volume), then putting the second Li electrode (450 µm thickness, 17 mm diameter), a 1 mm thick stainless steel spacer (16 mm diameter) on top, and finally adding the washer and crimping the cell inside the glove box. As argued previously, the larger separator size (compared to the electrode area) avoids stray currents around the separator, and the thick (500 µm), incompressible separator ensures sufficiently long relaxation times after the current pulses.[5]

The pulse experiments of two cells for each electrolyte concentration were conducted outside the glove box in a temperature controlled climate chamber (PR15, ThermoTEC, Germany) at temperature set-points of −10°C to 50°C (in 10°C steps), i.e., different temperatures were measured using the same cell. Unfortunately, the real cell temperatures were found later to differ from the set-point values, predominantly at low temperatures, so that the actual measurement temperatures were −7.5°C, +2.5°C, +12°C, +20°C, +30°C, +40°C, and +50°C (all ±1°C). For the calculation of the binary diffusion coefficients we used the measured temperatures and plot the data accordingly (see Figures 8d–8e). Even though the analysis scheme (see Theory section and Figure 1) requires identical measurement temperatures for concentration cell and coin cell experiments, we neglected the slight temperature differences at temperatures below +20°C and used the set-point temperatures for our calculation of the transport factor $b(c_0)$. It should be noted therefore, that this might compromise the precision of the transference number and the thermodynamic factor evaluated at temperatures below +20°C. Specifically, for the calculation of the transport factor $b(c_0)$ at, e.g., −10°C, the diffusion coefficient measured at −7.5°C is used, corresponding to an overestimation by ∼6% (based on finally obtained temperature dependent diffusion coefficient). Analogously the potential at current interrupt is underestimated by 4% (based on the extrapolation of $U(T_I)$ vs. *T* in the temperature range from 20°C to 40°C to −10°C). In omitting these inaccuracies, the evaluation of $b(c_0)$ at −10°C with $D_\pm$ and $U(T_I)$ yields a 1% lower value compared to the temperature corrected analysis with 0.94 x $D_\pm$ and 1.04 x $U(T_I)$; therefore, the slight temperature inaccuracy is neglected in the analysis. Measurement conditions for the pulse experiments, conducted with a Biologic VMP3 potentiostat, are listed in Table I. The duration for the galvanostatic pulses is chosen to ensure that concentration gradients are only forming at the vicinity of the electrodes (the maximum diffusion length during a 15 minute pulse under the here investigated conditions is ∼850 µm (based on (900 s × $8 \cdot 10^{-6}$ $cm^2/s)^{0.5}$), while the effective length through the porous medium with a tortuosity of 4.8 (see below) is 500 µm × 4.8 ≈ 2500 µm.

Table I. Summary of the applied galvanostatic pulse polarization (GPP) steps for different measurement temperatures for all $LiPF_6$ concentrations in the Li-Li coin cell setup shown in Figure 1. The active electrode area in the coin cells was 2.27 cm^2, i.e., 100 µA correspond to ∼45 µA/cm^2. Electrochemical impedance spectroscopy (EIS) measurements were conducted before each pulse (200 kHz - 1 Hz, with an amplitude of 10 mV).

Set Temp.	OCV + EIS	GPP	OCV
−10°C	EIS measurement + 1 h for temperature equilibration	15 min, ± 100 µA	3 h 45 min measured every 3 s
0, 10, 20, 30, 40°C	EIS measurement + 1 h for temperature equilibration	15 min, ± 300 µA	3 h 45 min measured every 3 s
50°C	EIS measurement + 1 h for temperature equilibration	15 min, ± 500 µA	3 h 45 min measured every 3 s

Alternating positive and negative pulse currents below 0.3 mA/cm^2 were chosen on purpose in order to avoid the unidirectional growth of lithium dendrites, and all pulses were followed by ∼4 h open circuit voltage measurement. The measurement procedure was set up to take 5 h, so that for each electrolyte and concentration the temperature was held for 10 h to accommodate two pulses (positive and negative current). After the pulse experiment at 50°C, the cell was cooled down to 20°C and a final pulse experiment was conducted to be compared to the initial 20°C measurement during the increasing temperature cycle. Within the error bars (see Section Results), no influence of the pulse direction could be observed, while repeat measurements at 20°C at the end of the procedure yielded slightly lower diffusion coefficients (max. 10% lower), but still within the measurement uncertainty of the first 20°C measurements.

In addition to the pulse experiments, four separate coin cells were prepared analogously (incl. metallic lithium) for the determination of the Nitto separator tortuosity $\tau_{Sep.}$, using both 1.0 M and 2.0 M $LiPF_6$ in EC:EMC (3:7, w:w), measuring their impedance response at temperatures of −10°C, 0°C, +25°C, +40°C, and +50°C. An average tortuosity of 4.8 ± 0.4 was found for the plasma treated Nitto film separator by analysis of the high frequency resistance, using the temperature dependent electrolyte conductivities that have been determined beforehand using the setup described above (see Conductivity Cell Design and Measurements). As expected, the measured tortuosity was independent of salt concentration and temperature, and the value of $\tau_{Sep.} = 4.8$ was used throughout this study for the calculation of the binary diffusion coefficient.[1]

Theory

Fundamental considerations for the analysis.—In the following, we briefly guide through the determination methods used in this work to obtain the transport properties of binary lithium-ion battery electrolytes, required for the application of the Newman model.[4] The Newman model describes the mass and energy conservation of a binary electrolyte by

$$\varepsilon\frac{\partial c}{\partial t} - \nabla\cdot\left(\frac{\varepsilon}{\tau}D_{\pm}(c)\nabla c\right) + \nabla\cdot\left(\frac{t_+(c)}{z_+\nu_+F}\vec{i}\right) = 0 \qquad [1]$$

$$\vec{i} = -\frac{\varepsilon}{\tau}\kappa(c)\ \nabla\Phi + \frac{\nu_+ + \nu_-}{z_+\nu_+} \cdot\frac{RT}{F}\frac{\varepsilon}{\tau}\kappa(c)\left[1 + \frac{d\ln f_{\pm}(c)}{d\ln c}\right](1 - t_+(c))\frac{1}{c}\nabla c \qquad [2]$$

according to the nomenclature summarized in the List of Symbols in the Appendix.

Figure 1 graphically summarizes the transport parameter determination scheme used in this study and depicts the experimental setups. Properties fixed by the experimental conditions and materials (colored in blue) and the quantities determined from the experiments (colored in red) are marked to allow for an easy distinction. The latter are the high frequency resistance in the conductivity cell R_{HFR}, the concentration potential in the concentration cell U_{CC}, the slope of the logarithm of the OCV relaxation vs. time for long times after a galvanostatic pulse applied to a symmetric Li-Li cell m_{ln}, and the potential $U(T_1)$ obtained just after the current interrupt upon a galvanostatic pulse for the time T_1, are marked to allow for an easy distinction.

The measurement of the ionic conductivity is rather straightforward and was done using turn-key equipment (see Figure 1, left panel). After finding the cell constant of the conductivity cell (k_C) using three conductance standards, the high frequency resistance R_{HFR}, obtained by electrochemical impedance spectroscopy (EIS) measurements of the cell filled with the electrolyte of interest, is used to calculate the electrolyte's ionic conductivity κ (see Figure 1, left panel).

The determination of the binary diffusion coefficient was described in detail in a previous publication and is applied analogously in this work.[5] While minor changes in the experimental setup and the measurement procedure are described in the Experimental section (separator type, cell setup), the approach used in this study for the measurement of binary diffusion coefficients is based on the analysis of the long-term potential relaxation after a galvanostatic polarization (see right panel in Figure 1 or Eq. 14 in Ref. 5). In a symmetrical Li-Li cell with an active electrode area $A_{El.}$, separated by a porous separator (thickness $l_{Sep.}$, porosity $\varepsilon_{Sep.}$) and filled with the electrolyte of interest (concentration c_0), the slope of the logarithm of the potential vs. time, m_{ln}, obtained at long times after the current interrupt allows to determine the partial effective binary diffusion coefficient $D^*_{\pm,eff}(c_0)$

$$D^*_{\pm,eff}(c_0) \equiv D_{\pm}(c_0)/\tau_{Sep.} = \frac{l_{Sep.}^2}{\pi^2}\cdot m_{ln}. \qquad [3]$$

From this, the binary diffusion coefficient $D_{\pm}(c_0)$ can be obtained if the tortuosity of the porous separator $\tau_{Sep.}$ is known (as quantified above).[5]

Previously, we suggested to find transference numbers (t_+) from concentration cell potentials when combined with a known thermodynamic factor (see Eq. 38 in Ref. 6)

$$t_+(c_0 \pm \delta c) \approx 1 - \frac{z_+\nu_+}{\nu}\frac{F}{RT}U\left[\int_{c_0-\delta c}^{c_0+\delta c}\mathrm{TDF}(c)\mathrm{d}(\ln c)\right]^{-1} \qquad [4]$$

This was based on our believe that we would be able to directly quantify the thermodynamic factor from an analysis of the ferrocene/ferrocenium redox potential versus a metallic lithium reference electrode by means of cyclic voltammetry,[7] whereby the thermodynamic factor (TDF) is defined as the following relationship between the mean molar activity coefficient $f_{\pm}$ of a salt and the salt concentration:

$$\mathrm{TDF} = 1 + \frac{d\ln(f_{\pm})}{d\ln(c)} \qquad [5]$$

Unfortunately, we have recently realized that one of the basic assumptions made in our previous publication on the determination of thermodynamic factor (TDF) via the ferrocene/ferrocenium approach[7] is not necessarily fulfilled, so that the determined TDF is not reliable (for details see the corresponding erratum[19] to Reference 7). Therefore, we here instead use concentration cell data in combination with the analysis of the short-time OCV relaxation after a galvanostatic pulse in symmetric Li-Li cells to quantify the temperature and concentration dependent behavior of the thermodynamic factor and the transference number. The determination method is similar to the methodology introduced before (see Eq. 10 or Eq. 26 in Ref. 6), which is based on the short-term OCV analysis of galvanostatic pulse experiments in symmetrical Li-Li cells in combination with the measurement of concentration cell potentials. However, here we will introduce a modification of that measurement methodology which facilitates the direct extraction of concentration dependent values of TDF and t_+.

In order to do so, we first introduce a further simplification to the analysis of concentration potentials (see Figure 1, middle panel), which reduces the complexity and the ambiguity of the data analysis. In concentration cells with two identical electrodes (here metallic lithium) in contact with two electrolytes which differ sufficiently little in their salt concentrations (i.e., differing from a base concentration c_0 by a value of $\pm\Delta c$), the concentration cell potential U_{CC} for a binary electrolyte with a 1:1 salt (e.g., $LiPF_6$) can be described by[4,6]

$$U_{CC} = \frac{2RT}{F}\int_{c_0-\Delta c}^{c_0+\Delta c}\left(\frac{1}{c}\mathrm{TDF}\,(c)\cdot(1-t_+\,(c))\right)\mathrm{d}c \qquad [6]$$

and may be simplified to

$$U_{CC} = \frac{2RT}{F}\mathrm{TDF}\,(c_0)\cdot(1-t_+\,(c_0))\int_{c_0-\Delta c}^{c_0+\Delta c}\frac{1}{c}\,\mathrm{d}c \qquad [7]$$

$$U_{CC} = \frac{2RT}{F}\mathrm{TDF}\,(c_0)\cdot(1-t_+\,(c_0))\ln\left(\frac{c_0+\Delta c}{c_0-\Delta c}\right) \qquad [8]$$

under the assumption of a constant transference number and a constant thermodynamic factor between the two differential concentrations $c_0-\Delta c$ and $c_0+\Delta c$. Here, R is the gas constant, F the Faraday constant, and T the temperature. While this assumption is only strictly valid for infinitely small concentration intervals, it provides a good approximation if reasonably small concentration differences are used and if the transference number and the thermodynamic factor are well behaved in the considered concentration range of $c_0\pm\Delta c$. Once the thus determined functional approximations of $\mathrm{TDF}(c_0)$ and $t_+(c_0)$ from the experimental data are determined, the error of the above simplification can be checked mathematically by comparing the concentration potentials U_{CC} obtained from Eq. 6 vs. that from Eq. 8. For the individual trends of $\mathrm{TDF}(c_0)$ and $t_+(c_0)$ at different temperatures and for different electrolytes obtained in the following (Figure 9 and Figure 10), the error introduced by the simplified Eq. 6 was found to be below 10% for all measurements (see Supporting Information Figure 3). In consequence, rearrangement of Eq. 8 allows to determine the transport factor $a(c_0)$, which contains the thermodynamic factor $\mathrm{TDF}(c_0)$ and the term $(1-t_+(c_0))$ for the arithmetic mean salt concentration c_0:

$$a\,(c_0) \equiv \mathrm{TDF}(c_0)\cdot(1-t_+\,(c_0)) = \frac{F\cdot U_{CC}}{2\,R\,T}\cdot\frac{1}{\ln\left(\frac{c_0+\Delta c}{c_0-\Delta c}\right)} \qquad [9]$$

Here it should be noted that although the logarithmic concentration mean would be mathematically more precise compared to the arithmetic mean salt concentration c_0, it only introduces a minor correction for the small concentration pairs and is neglected here.

In addition to the concentration cell potentials, the pulse relaxation in symmetric Li-Li cells is analyzed. Specifically, the short-term potential relaxation after galvanostatic pulses in symmetric Li-Li cells (see Eq. 26 in Ref. 6, with $z_+ = 1$, $\nu_+ = 1$, and $\nu = 2$) allows to obtain the relationship

$$\mathrm{TDF}(c_0)\cdot\frac{(1-t_+\,(c_0))^2}{\sqrt{D^*_{\pm,\mathrm{eff}}}} = \frac{\sqrt{\pi}}{8}\frac{F^2}{R\,T}A_{\mathrm{El.}}\cdot\varepsilon_{\mathrm{Sep.}}\cdot c_0\frac{U\,(T_I)}{I_p\sqrt{T_I}} \qquad [10]$$

where $U(T_I)$ is the open circuit voltage established just after the interruption of the current pulse which was applied for a duration time T_I, i.e., directly after application of the constant current I_P. As described before, $U(T_I)$ can be obtained by linear extrapolation of the potential versus a normalized time-scale, viz., versus $1\text{-}\tau^*$, where the transformed time variable τ^* is defined as $\frac{\sqrt{T_I}}{\sqrt{t+\sqrt{t-T_I}}}$ (note that t denotes the time from the beginning of the pulse).[6,20] Knowing the relation of the partial effective binary diffusion coefficient with the slope of the logarithmic potential relaxation for long times (see Eq. 3), allows to rewrite Eq. 10 to yield another transport factor $b(c_0)$.

$$b\,(c_0) \equiv \mathrm{TDF}(c_0)\cdot(1-t_+\,(c_0))^2$$
$$= \sqrt{\frac{\left(l_{\mathrm{Sep.}}\right)^2}{\pi^2}\cdot m_{\ln}}\cdot\frac{\sqrt{\pi}}{8}\frac{F^2}{R\,T}A_{\mathrm{El.}}\cdot\varepsilon_{\mathrm{Sep.}}\cdot c_0\frac{U\,(T_I)}{I_p\sqrt{T_I}} \qquad [11]$$

If the, herein called, transport factors $a(c_0)$ and $b(c_0)$ are determined for the same base concentration c_0 and the same temperature T, simple arithmetic allows to determine both the thermodynamic factor and the transference number (see Figure 1, lower horizontal panel). While this determination scheme has the advantage of requiring only two measurements (concentration cell and pulse polarization), it cannot be used to independently determine individual values for either TDF or t_+ from just one experiment (as is the case for $D_\pm$), so that the quantification of TDF and t_+ requires a combination of two independent measurements in different cell setups, which in turn intrinsically increases the experimental error of the determined TDF and t_+ values. In the Data Analysis section, we will show representative, exemplary datasets and their analysis, so that the reader is able to follow step by step how to obtain the final values and their errors (see Data Analysis section. Error calculation and regression analysis in the supporting information), presented in the Results section.

Data Analysis

In the following, we will present exemplary data and depict the data analysis used to obtain the transport properties shown in the subsequent Results section. In a step by step process, we guide the reader through the data treatment which follows the outline sketched in Figure 1 and we describe difficulties observed during the measurements. This is done in such detail, as we believe that correct interpretation and evaluation of the found concentration and temperature dependencies of the electrolyte parameters is only possible when the analysis steps are well understood.

Conductivity measurements.—Figure 2 shows exemplary Nyquist plots of the EIS data in the conductivity measurement cell for 1.0 M $LiPF_6$ in EMC:FEC (19:1 w:w) at temperatures from −10°C to +50°C. The impedance spectra recorded in a frequency range from 85 kHz to 1 kHz with an excitation amplitude of 100 mV show a similar behavior, i.e., a partially visible semicircle at high frequencies followed by a linear capacitive branch at low frequencies. For the extraction of the cell resistances, each individual spectrum was fitted automatically with a custom implementation of the modulus weighing[21] in Matlab, employing the *fminsearch* algorithm.[22] For this, an equivalent circuit is used consisting of an R/Q element (parallel circuit of a resistor and a constant phase element) to account for the partially visible, depressed high frequency semicircle (from the ionic resistance of the electrolyte and the cell's geometrical capacitance) and a serially connected constant phase element to describe the capacitive behavior (from the double layer capacitance at the electrode/electrolyte interfaces); the phase angle of the latter is slightly below 90° (apparent by the not perfectly vertical line at low frequencies in Figure 2). Fits of the R/Q + Q equivalent circuit model to the experimental data are found to be in excellent agreement with the data and are depicted as solid lines in Figure 2. Analysis of the fitting parameters allows to extract the resistance value R_{HFR} (depicted as circles on the x-axis in Figure 2, with colors representing measurement temperatures according to the legend), corresponding to the ionic resistance of the electrolyte at the given current temperature. Ionic conductivities are then obtained with the cell constant ($k_C = 20 \pm 0.2$ 1/cm) determined using three conductance standards (see Experimental section), and are summarized in Figures 8a–8c for all electrolytes, concentrations, and temperatures. Error bars for the ionic conductivity correspond to 3 % to account for the error of the cell constant, the accuracy of the cell filling, and the fitting error. The obtained conductivities as well as their temperature and concentration dependence are discussed together with all other transport factors in the Results section.

Concentration cell measurements.—With the setup used in this work, measurement of the concentration potentials in the pouch concentration cells was only sufficiently accurate, as long as the two concentrations used yielded concentration cell potentials that were above 15 mV at all temperatures (see Figure 3). Thus, in contrast to the measurement scheme in the Theory section (Figure 1), where

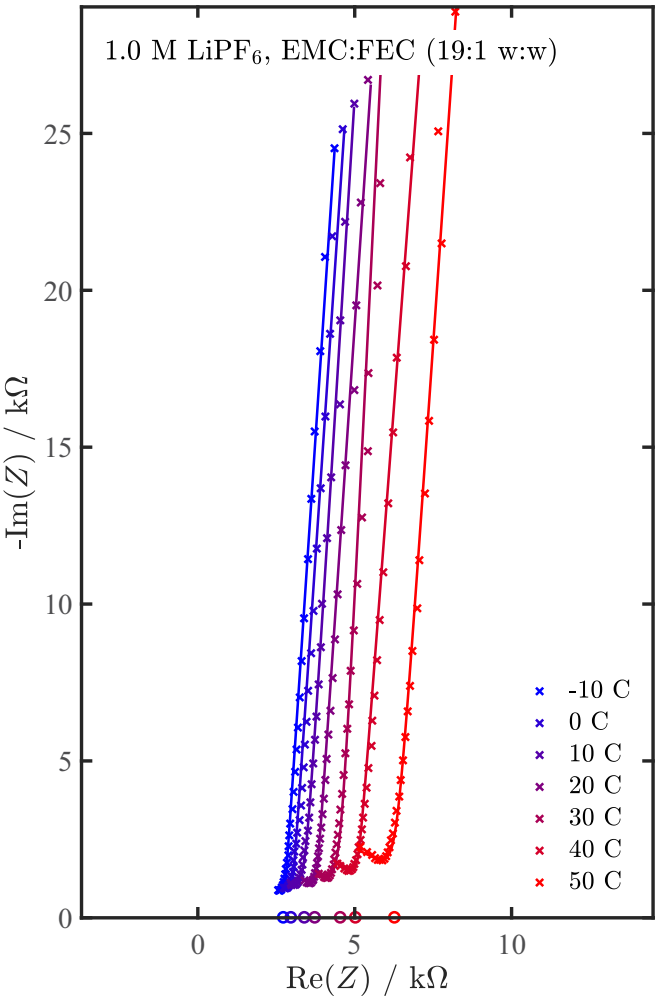

Figure 2. Exemplary EIS data (1.0 M $LiPF_6$ in EMC:FEC, 19:1 w:w) for the temperature dependent determination of ionic conductivity of 1 M $LiPF_6$ in EMC:FEC (19:1 w:w) from −10°C to +50°C, measured in the conductivity cell (with $k_C = 20 \pm 0.2$ 1/cm). EIS data (from 85 kHz to 1kHz, with 100 mV excitation amplitude) are indicated by crosses, the fit to the equivalent circuit (R/Q + Q) is shown as solid lines, and the extracted resistance values R_{HFR} are marked on the x-axis (open circles). The different colors indicate different measurement temperatures, as described by the legend.

concentrations of $c_0 \pm \Delta c$ are discussed, the concentrations used with the pouch concentration cells in this work are not symmetrically chosen around the main concentrations used in this work (0.1, 0.5, 1.0, 1.5, 2.0, 3.0 M $LiPF_6$), but we instead use adjacent base concentration pairs of 0.01–0.1, 0.1–0.5, 0.5–1.0, 1.0–1.5, 1.5–2.0, and 2.0–3.0 M $LiPF_6$ in the respective solvents. The rationale behind the enlarged concentration ratios is the insufficient signal to noise ratio for smaller concentration potentials. Especially with the pouch concentration cell setup (see Concentration Cell Design and Measurements in the Experimental section), the large distance between the electrodes ($d_{Sep.} = 10$ cm), the high tortuosity and low porosity of the separator ($\tau_{Sep.} = 4.8$, $\varepsilon_{Sep.} = 30\%$; see Experimental section), coupled with the low ionic conductivity (on the order of $k \approx 1$ mS/cm for low salt concentrations and temperatures) will yield very high cell resistances of up to 3 MΩ:

$$R_{CC} = \frac{d_{Sep.} \cdot \tau_{Sep.}}{\kappa \cdot A_{Sep.} \cdot \varepsilon_{Sep.}} = \frac{10\,\text{cm} \cdot 4.8}{1\,\frac{\text{mS}}{\text{cm}} \cdot (500\,\mu\text{m} \cdot 1\,\text{cm}) \cdot 0.3} \approx 3\,\text{M}\Omega \quad [12]$$

Here the cross-sectional area of the separator $A_{Sep.}$ is based on a width of 1 cm and a thickness of 500 μm. Precise open circuit voltage measurements of such highly resistive cells are very noise sensitive and would require specialized equipment, which manifested itself in our measurements by high noise levels when walking by the setup or when the circulator of the cooling/heating bath was running. For that reason, the circulator was completely switched of during the measurement period (3 min), during which time the temperature however remained very stable (the temperature difference prior to switching off and turning on the circulator was <0.5°C).

Figure 3 shows the concentration cell potentials for all electrolyte solutions, specifying the used concentrations next to the data inside the figure. The observed concentration potentials range between 19 ± 2 mV (for 0.5–1.0 M $LiPF_6$ in EMC:FEC (19:1 w:w) at −10°C, see pink squares in Figure 3c) and 105 ± 2 mV (for 2.0–3.0 M $LiPF_6$ in EC:DMC (1:1 w:w) at −10°C, see brown squares in Figure 3a). For each concentration and temperature, at least two cells were measured and the error bars are calculated according to the section 4. Error calculation and regression analysis in the supporting information using the mean potential during the measurement period as x_i and its standard deviation as Δx_i. Concentration potentials were found to depend fairly linearly on temperature (linear trend lines are added in Figure 3 as a guide-to-the-eye). While for high concentrations the concentration overpotential decreases with increasing temperatures (by ∼10–20% from −10°C to +50°C, see brown squares/lines in Figure 3), this trend mostly reverses for lower concentrations (see turquoise and orange squares/lines in Figure 3). The generally small temperature dependence of the concentration potentials observed in Figure 3 for all concentration ranges and electrolytes illustrates why reasonably large concentration differences are required to extract a numerically significant variation of U_{CC} with temperature (this constraint could possibly be relaxed if a more precise voltage measurement device would be used).

As explained in the Theory section, it is advantageous to convert the measured concentration potentials into the transport factors $a(c_0)$ (≡ $\text{TDF}(c_0) \cdot (1 - t_+(c_0))$) by assuming a constant TDF and a constant transference number between the two electrolyte concentrations used in the pouch concentration cells (see Eq. 9). From the thus obtained temperature and concentration dependent transference number and thermodynamic factor, the error due to the simplification of the integral was tested by comparison of Eq. 6 and Eq. 8, whereby the difference between both was found to be below 10% (see Supporting Information, Figure 3). Figure 4 shows the transport factors a, calculated from the concentration potentials in Figure 3 (square symbols, with colors corresponding to the temperature, see legend in the figure). Here, the calculated a-values are plotted vs. the arithmetic mean concentration of the respective electrolyte concentration pair (e.g., a for 1.5–2.0 M $LiPF_6$ is plotted at $c = 1.75$ M). The general behavior of a with temperature and concentration is found to be similar for the three examined electrolytes. At mean concentrations of 0.055 M (mean between 0.01 M and 0.1 M electrolytes) and for all temperatures, values between 0.3 and 0.6 are obtained, which increase with increasing salt concentrations (to $a = 3.5$–6 for a mean concentration of 2.5 M, i.e., the mean of 2.0 M and 3.0 M $LiPF_6$), at which point the decrease of a with increasing temperature becomes more prominent. When comparing the transport factor a reported in the literature for $LiPF_6$ in EC:EMC (3:7 w:w) at 25°C (from Figure 9 in Ref. 23) to our measurements for the same electrolyte (at 20°C and 30°C), an excellent agreement can be found (see solid black line in Figure 4b). Additionally, although not representing exactly the same electrolyte composition, we depict the transport factor a for $LiPF_6$ in PC (propylene carbonate):EC:DMC (10:27:63 v:v:v) reported by Valøen and Reimers[8] in the temperature range from −10°C (blue line, upper limit) to +50°C (red line, lower limit) as the gray shaded area in Figure 4a (from Figure 6 in Ref. 8). While the trends agree well at low concentrations, for increasing $LiPF_6$ concentration the transport factor a found by Valøen and Reimers remains at lower values (on average 4 at 2.5 M compared to 5 for our measurements), likely due to the different electrolyte composition which includes PC.

In their publication, the authors find that their fit of the transport factor a is independent of temperature at low concentrations (as also observed in Figure 4), from which they conclude that the transference

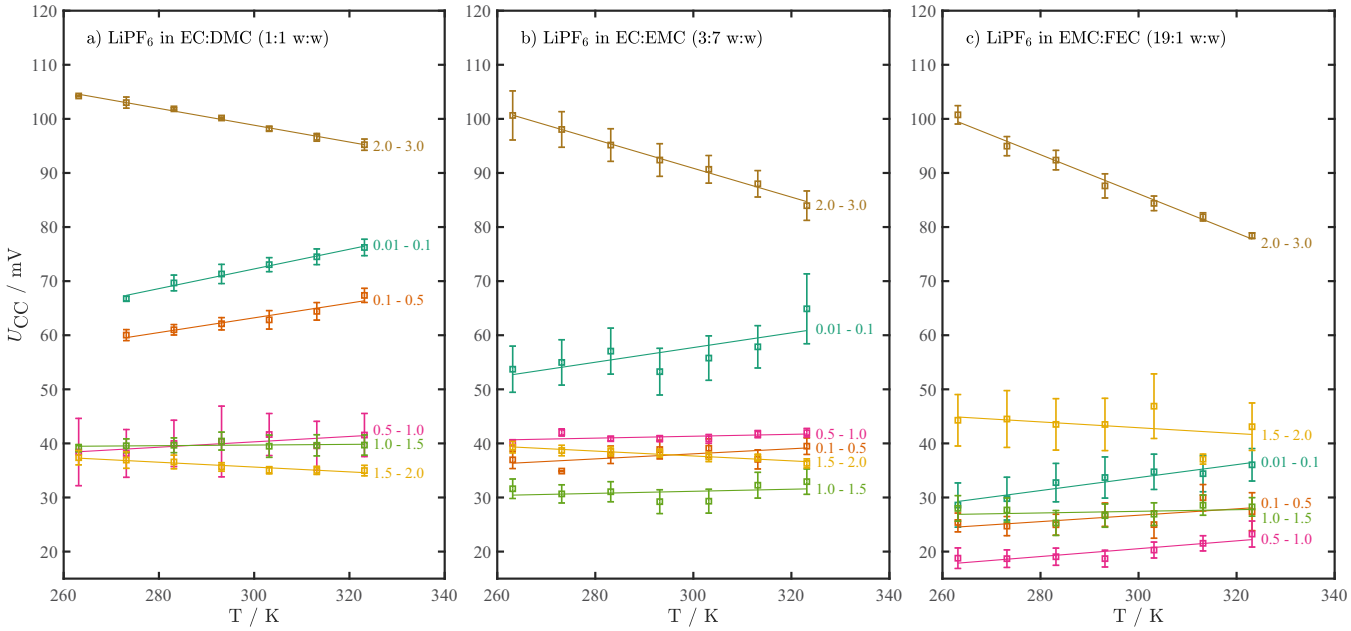

Figure 3. Concentration potentials U_{CC} (averaged over 3 min) measured in pouch concentration cells between identical electrolytes with different $LiPF_6$ concentrations (specified in the figure), for temperatures ranging from −10°C to +50°C: a) EC:DMC (1:1 w:w), b) EC:EMC (3:7 w:w), and, c) EMC:FEC (19:1 w:w). Errors are calculated as explained in the section 4. Error calculation and regression analysis in the supporting information, with the mean potential during the measurement period as x_i and its standard deviation as Δx_i, whereby at least two cells were measured for each configuration. The temperature was controlled using a refrigerated/heated circulator bath (switched off during measurement) and the measurements were conducted by immersing the pouch cells into the bath.

number must be temperature invariant at low concentrations, because the thermodynamic factor is defined as 1 for $c \to 0$. This conclusion, however, can hardly be verified, as their experimental concentration cell data are only shown for one temperature (at 21°C, see Figure 5 in their publication) and as the smallest concentrations pairs in their study extend over a very wide range (77 µM to 0.4 M). This large concentration difference in the small concentration region does not allow to resolve the Debye-Hückel behavior, which theoretically predicts a strong change of the TDF with temperature at low concentrations, due to the temperature dependence of the relative permittivity of the solvent.[24] To prove the temperature invariance of the transference number at low concentrations hypothesized by Valøen and Reimers, much smaller concentration differences in the small concentration range (<0.1 M) and more measurements would be required. One must also consider that a nearly temperature invariant transport factor a does not necessitate a temperature independence of the transference number,

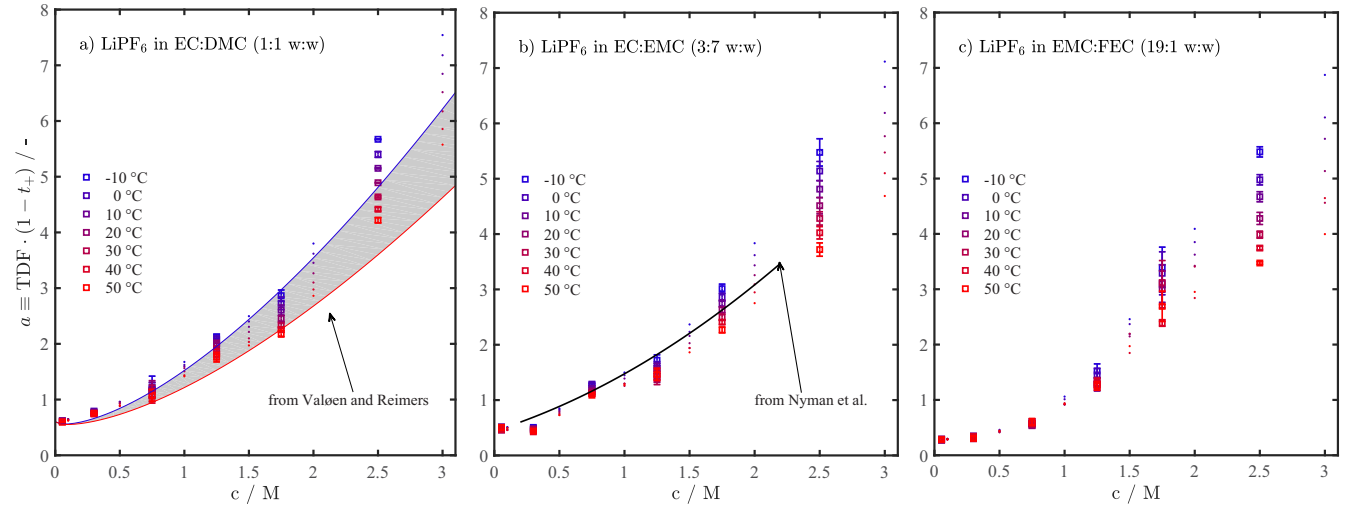

Figure 4. Transport factor $a(c_0) \equiv \mathrm{TDF}(c_0) \cdot (1 - t_+(c_0))$ vs. the mean molar $LiPF_6$ concentration and temperature (−10°C to +50°C; indicated by the color scheme in the figure), as calculated from the concentration potentials shown in Figure 3 using the approach discussed in the Theory section (see Eqs. 6–9), for: a) EC:DMC (1:1 w:w), b) EC:EMC (3:7 w:w), and, c) EMC:FEC (19:1 w:w). Data points are shown at the arithmetic mean concentration of the concentration cell setup (squares); also included are linear inter-/extrapolation points to the base concentrations used in this work (0.1, 0.5, 1, 1.5, 2.0, and 3.0 M $LiPF_6$; depicted as dots). Additionally depicted are the transport factors a reported in the literature: in Figure 4a for $LiPF_6$ in PC:EC:DMC (10:27:63 v:v:v)[8] (gray shaded area with the blue line as upper limit at −10°C and the red line as lower limit at +50°C) and in Figure 4b for $LiPF_6$ in EC:EMC (3:7 w:w) at 25°C[23] (solid black line). Errors are calculated as explained in the section 4. Error calculation and regression analysis in the supporting information with the individual a values from repeat cells as x_i and their uncertainty, based on the standard deviation of the concentration potential during the measurement time, as Δx_i; at least two cells were measured for each configuration.

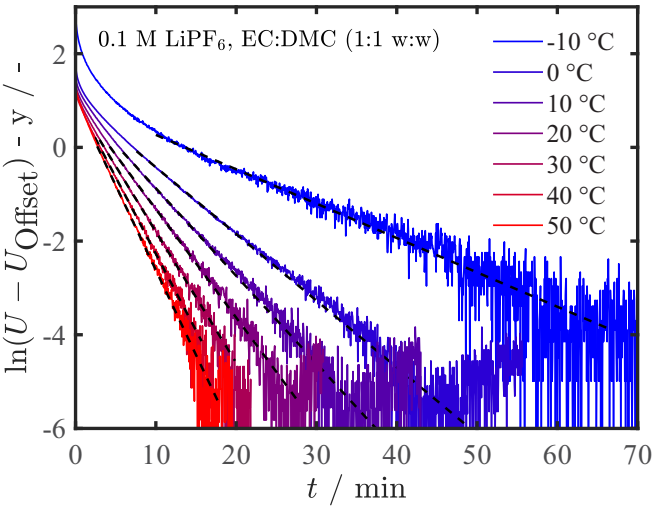

Figure 5. Exemplary potential relaxation data for the temperature dependent (−10°C to +50°C) determination of the binary diffusion coefficient in EC:DMC (1:1 w:w) with 0.1 M $LiPF_6$, measured in symmetrical Li-Li coin cells with a plasma treated Nitto separator (see Experimental section for setup details and Table I for the measurement procedure). The measured potentials are corrected by the final offset potential (mean of the last 5 min, with $|U_{offset}|$ always <1 mV) and the term $\ln(U\text{-}U_{offset})$ is shifted so that the linear trend lines start at a y-axis value of 1. Time ranges for the linear trend lines (shown as black dashed lines) are selected automatically (see text). Colors represent measurement temperatures as described by the figure legend; the reader is referred to the Experimental section for details on the precise measurement conditions.

since, e.g., similar but in sign opposite temperature dependencies of TDF and t_+ could also result in a temperature invariant a-value (remember $a(c_0) \equiv \mathrm{TDF}(c_0) \cdot (1 - t_+(c_0))$).

Additionally shown in Figure 4 are linearly inter- and extrapolated points at the base concentrations used in this work, i.e., at 0.1, 0.5, 1.0, 1.5, 2.0, and 3.0 M $LiPF_6$, which are necessary to follow the analysis scheme introduced in the Theory section (see Figure 1), as will be explained below. The reader is reminded that in this work it was necessary to use enlarged concentration ranges for the measurement of concentration potentials, due to the high cell resistances and the associated noise-prone voltage measurements. An optimization of the voltage measurement setup to more accurately determine concentration cell potentials might enable the use of more closely differential concentrations around the base concentrations of interest, so that one can exactly follow the measurement scheme in Figure 1 which would obviate the need for inter- and extrapolation.

Based on Figure 4, one may be tempted to draw first conclusions on the absolute values of the transference number at infinite dilution. As already discussed above, since the mean molar activity coefficient as well as the thermodynamic factor are 1 at infinite dilution, the transference number at infinite dilution could be estimated from the a-value at the lowest concentration range. However, because the smallest mean $LiPF_6$ concentration in Figure 4 is already 55 mM (arithmetic mean of 10 and 100 mM) and since the Debye Hückel behavior of the activity coefficient suggests a steep decrease from 1 to smaller values in already much smaller concentration ranges,[25] we believe that no reliable estimates of t_+ at infinite dilution can be obtained from the data in Figure 4, so that we refrain from this type of analysis in order not to mislead the reader.

Pulse experiments.—To obtain the binary diffusion coefficient as well as the transport factor $b(c_0) \equiv \mathrm{TDF}(c_0) \cdot (1 - t_+(c_0))^2$, see Figure 1), which is necessary to deconvolute transference number and thermodynamic factor which are coupled in the above determined transport factor a, pulse experiments in symmetric Li-Li coin cells were conducted (see Experimental for measurement procedure and Figure 1 for cell setup). For each base concentration (0.1, 0.5, 1.0, 1.5, 2.0, and 3.0 M $LiPF_6$) of the three different electrolyte solvent mixtures (EC:DMC (1:1 w:w), EC:EMC (3:7 w:w), and EMC:FEC (19:1 w:w)), two coin cells were built; for a detailed overview of the measurement procedure, the reader is referred to Table I in the Experimental section.

In the following, we first show exemplarily the determination of the binary diffusion coefficient, based on the long-term potential relaxation after galvanostatic pulses (for details on the method, the reader is referred to Ref. 5). In this work, the binary diffusion coefficient is obtained from the slope of the logarithm of the potential relaxation at long times after the current interrupt. As an example, Figure 5 shows the logarithm of the potential measured after application of the second (negative) current pulse in symmetric Li-Li cells containing 0.1 M $LiPF_6$ in EC:DMC (1:1 w:w) at temperatures from −10°C to +50°C (see Experimental section for the precise temperatures). Even in the long-time limit the potential of the coin cells did not relax to exactly zero mV, but a finite offset potential U_{Offset} remained (typically between 0 and <+|1 mV|), which was subtracted from the measured potentials. In this work, U_{Offset} is taken as the mean of the last 100 points (= last 5 min) recorded during the relaxation period of 3.75 h. The ranges over which the linear trend lines were fitted are marked for each temperature in Figure 5 (see dashed black lines) and were selected as follows. Due to a finite noise level of the potential measurement (∼0.3 mV), we defined the end point for the linear trend lines as the time for which the measured potential dropped below 0.3 mV for the first time (with U_{Offset} subtracted from the experimental data beforehand). The start time for linear extrapolation was chosen as 15% of the time at which the end point was reached. Because different pulse currents were applied for different temperatures (see Table I) in order to maximize the signal to noise ratio without driving too much lithium plating, the absolute starting potentials vary and the y-axis values of the experimental data in Figure 5 are further shifted by y (chosen, so that the linear trend lines start at a y-axis value of 1) to enable a more straightforward comparison of the data at different temperatures. From the representative data shown in Figure 5, clear linear trend lines can be observed at all measured temperatures over reasonably long periods of time (∼10 to 60 min at +50°C to −10°C, respectively). It is noted that a relaxation time of ∼4 h (see measurement procedure in Table I) was necessary to allow for a full potential relaxation, especially for the concentrated electrolyte solutions and at low temperatures.

When the cell potential U (subtracted by U_{Offset}) approaches 0 mV, the logarithm of $(U\text{-}U_{offset})$ starts to show high scatter due to the finite measurement accuracy (see −10°C curve in Figure 5). To consider the effect of the selected time range for the linear trend line fit on the resulting slopes (m_{ln}), we also determine the linear trend lines for time ranges shifted by ±50% from the automatically selected lower time limit, i.e., three values for the slope m_{ln} are obtained which are used for the error calculation (see below). From the m_{ln}-values obtained from the trend lines, the separator thickness $l_{Sep.}$, and the separator tortuosity $\tau_{Sep.}$ (see Coin Cells in the Experimental section), the binary diffusion coefficient $D_\pm$ can be obtained for a given electrolyte and temperature (see Eq. 3). Weighted mean binary diffusion coefficients and their error are calculated from the positive and negative pulse experiments of both repeat cells according to the section 4. Error calculation and regression analysis in the supporting information, using the mean of the three $D_\pm$ values obtained from the three different time ranges as x_i and their standard deviation as Δx_i. The finally obtained binary diffusion coefficients and their temperature and concentration dependence for the electrolytes under study are summarized in Figure 8 and will be discussed in the Results section.

In addition to the direct determination of the binary diffusion coefficient from the long-term potential relaxation after the galvanostatic pulses in symmetric lithium cells, the short-time behavior of the potential directly after the current interrupt allows to determine the transport factor $b(c_0) \equiv \mathrm{TDF}(c_0) \cdot (1 - t_+(c_0))^2$, see Figure 1) by means of Eq. 11. The evaluation of Eq. 11 requires the known setup parameters (separator thickness $l_{Sep.}$ and porosity $\varepsilon_{Sep.}$, temperature T, salt concentration c_0, and active electrode area $A_{El.}$), the selected measurement characteristics (current pulse time T_I and magnitude I_P),

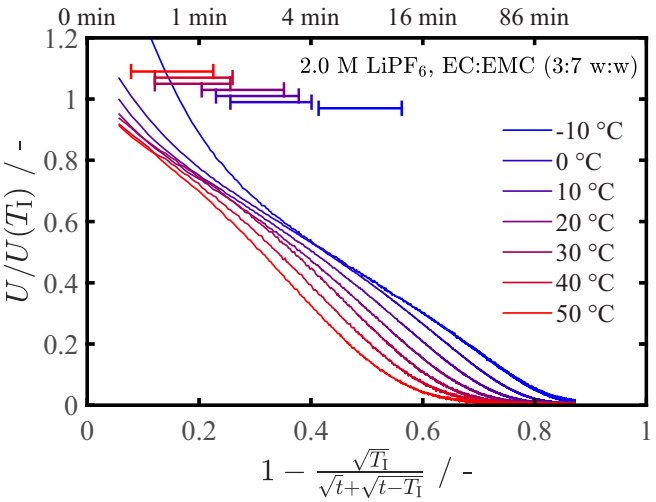

Figure 6. Exemplary potential transients vs. 1-τ* (τ* being the transformed time variable) upon a galvanostatic pulse (300 μA ≡130 μA/cm^2 for 15 min) recorded in symmetric Li-Li coin cells with a plasma treated Nitto separator, filled with 2.0 M $LiPF_6$ in EC:EMC (3:7 w:w) in the temperature range from −10°C to +50°C (see figure legend for details). The s-shaped curvature, as required for the application of the method,[6] is clearly visible at all measurement temperatures, while for short times deviations occur due to the reformation of the SEI (see blue curve at −10°C). The time intervals used for the linear extrapolation to the y-axis are shown above the potential transients (colors corresponding to measurement temperature). Real times are indicated at the top x-axis and correspond to the time after the current interrupt.

the above determined slope of the long-term potential relaxation $m_{\ln}$, and the yet to be determined potential $U(T_I)$ just following the end of the current pulse at $t = T_1$. Exemplarily we show the determination of $U(T_I)$ for the potential relaxation recorded in a symmetrical Li-Li coin cell filled with 2.0 M $LiPF_6$ in EC:EMC (3:7 w:w). Figure 6 shows the potential transients after the second (negative current) pulse recorded at temperatures from −10°C to +50°C, plotted versus 1 minus the transformed time variable τ* (i.e., vs. $1 - \frac{\sqrt{T_I}}{\sqrt{t}+\sqrt{t-T_I}}$).[6,20] To allow for a simple comparison, the potential values plotted in Figure 6 are normalized by the finally obtained potential immediately after the current interrupt $U(T_I)$. Figure 6 shows the typical s-shaped potential transients at all measured temperatures (see Figure 8a in Ref. 6), while the step appears later for lower temperatures. At −10°C (blue line), the step can be observed at $1 - \tau^* = 0.75$ (∼1 h after current interrupt), while for the 50°C measurement (red line) the step is clearly visible at already $1-\tau^* = 0.4$ (∼4 min after current interrupt). It has to be noted that the observation of the s-shape is a necessary requirement for the applicability of the analysis method, and its presence therefore further supports our experimental results.[6] Also visible in Figure 6 is the pronounced deviation from the theoretically expected linear behavior at short times (see upper inset in Fig. 2 of Ref. 6), which is most pronounced at low temperatures (see blueish curves in Figure 6) and might be caused by SEI reformation effects. As the potential of bare lithium metal and fully passivated lithium electrodes generally differ,[26] we would expect artefacts in the potential measurements until all lithium surfaces are fully covered with an SEI, the formation of which would happen more or less instantaneously at room temperatures and above, but may become slower at low temperatures. In contrast to the automated selection of the time range for the determination of the binary diffusion coefficient from the long-term potential relaxation, the time range (in terms of $1 - \tau^*$) for the linear extrapolation in Figure 6 to obtain $U(T_I)$ was selected manually. The center of the linear range at the beginning of the s-shaped potential transient, excluding the deviations at small times, was selected by eye and linear extrapolations were done using a time range of ±0.075 (in terms of $1 - \tau^*$) around that value. Although selected on an experiment by experiment basis, the selected center points generally lie close to $1 - \tau^* = 0.15$ for measurements at 50°C and around $1 - \tau^* = 0.5$ at −10°C, i.e., a consistent trend for the appearance of the step was found for all electrolytes under study. In Figure 6, the $1 - \tau^*$ ranges used for the linear extrapolation are shown as range bars above the potential transients (colors corresponding to measurement temperatures, see legend in the figure). The extrapolation of the measured potentials in the selected $1 - \tau^*$ ranges to the y-axis yields the potential at current interrupt $U(T_I)$ (unity in Figure 6 due to the above mentioned normalization of potentials). The uncertainty of the obtained $U(T_I)$ values is taken as the 95% confidence bounds, which are calculated using the *confint* function in Matlab.[22]

Analysis of the pulse experiments and extraction of the potentials at current interrupt times, as exemplarily shown for the electrolyte 2.0 M $LiPF_6$ in EC:EMC (3:7 w:w) in Figure 6, allows to calculate the corresponding transport factors $b(c_0) \equiv \mathrm{TDF}(c_0) \cdot (1 - t_+(c_0))^2$, see Figure 1) for each electrolyte, concentration, and temperature (see Eq. 11). In analogy to the above discussed analysis of the concentration overpotentials and the resulting values for the transport factor $a(c_0) \equiv \mathrm{TDF}(c_0) \cdot (1 - t_+(c_0)))$ in Figure 4, we summarize $b(c_0)$ for $LiPF_6$ in EC:DMC (1:1 w:w), EC:EMC (3:7 w:w), and EMC:FEC (19:1 w:w) in Figures 7a, 7b, and 7c, respectively. As before, values are calculated according to the section 4. Error calculation and regression analysis in the supporting information with the individual values for $b(c_0)$ (from positive and negative currents and two repeat cells) taken as x_i and their error, based on the confidence interval of $U(T_I)$, as Δx_i (note that we omit the error in $m_{\ln}$ here). The temperature and concentration dependence of $b(c_0)$ in Figure 7 closely resembles the behavior observed for the transport factor $a(c_0)$ in Figure 4, with increasing $b(c_0)$ values for higher concentrations and lower temperatures. For all electrolytes investigated in this study, steadily increasing $b(c_0)$ values are found from +50°C to 0°C. Measurements conducted at −10°C generally show an increased offset compared to the other temperatures, most pronounced at highest concentrations, which is generally accompanied by increased error bars in Figure 7; the origin of this is currently not understood.

Results

In the following, we will discuss the obtained concentration and temperature dependent transport and thermodynamic parameters of ionic transport in binary electrolytes obtained for the three here examined electrolytes. Ionic conductivities and binary diffusion coefficients are determined as outlined in the section Data Analysis. Transference numbers and thermodynamic factors are calculated for each concentration and temperature from the transport factors $a(c_0)$ and $b(c_0)$ (see Figure 4 and Figure 7) using the equations given in the scheme in Figure 1, i.e.,

$$t_+(c_0) = 1 - \frac{b(c_0)}{a(c_0)} \quad [13]$$

and

$$\mathrm{TDF}(c_0) = \frac{a(c_0)^2}{b(c_0)}. \quad [14]$$

Due to the necessity to measure the factor $a(c_0)$ for larger concentration differences to be able to detect temperature effects of the concentration potential U_{CC} (see Figure 3) and the consequently different mean concentrations (0.055, 0.3, 0.75, 1.25, 1.75 and 2.5 M $LiPF_6$) compared to the base salt concentrations used in this work (0.1, 0.5, 1.0, 1.5, 2.0 and 3.0 M $LiPF_6$), Eqs. 13 and 14 are always obtained from one measured (squares in Figure 4 and circles in Figure 7) and one interpolated (dots in Figure 4 and Figure 7) value of $a(c_0)$ and $b(c_0)$ or vice versa. For example, the thermodynamic factor of 1.0 M $LiPF_6$ in EC:DMC (1:1 w:w) at +40°C is obtained from the linearly interpolated transport factor $a(1.0\ \mathrm{M}) = 1.43$ (from a values at 0.75 M of 1.06 and at 1.25 M of 1.81) and the measured transport factor $b(1.0\ \mathrm{M})$ (0.75 measured at 1.0 M) by means of Eq. 14 to $\mathrm{TDF}(1.0\ \mathrm{M}) = 2.74$. Analogously, the transference number at 0.75 M for the same solvent and temperature is calculated with Eq. 13 using the measured transport factor $a(0.75\ \mathrm{M})$

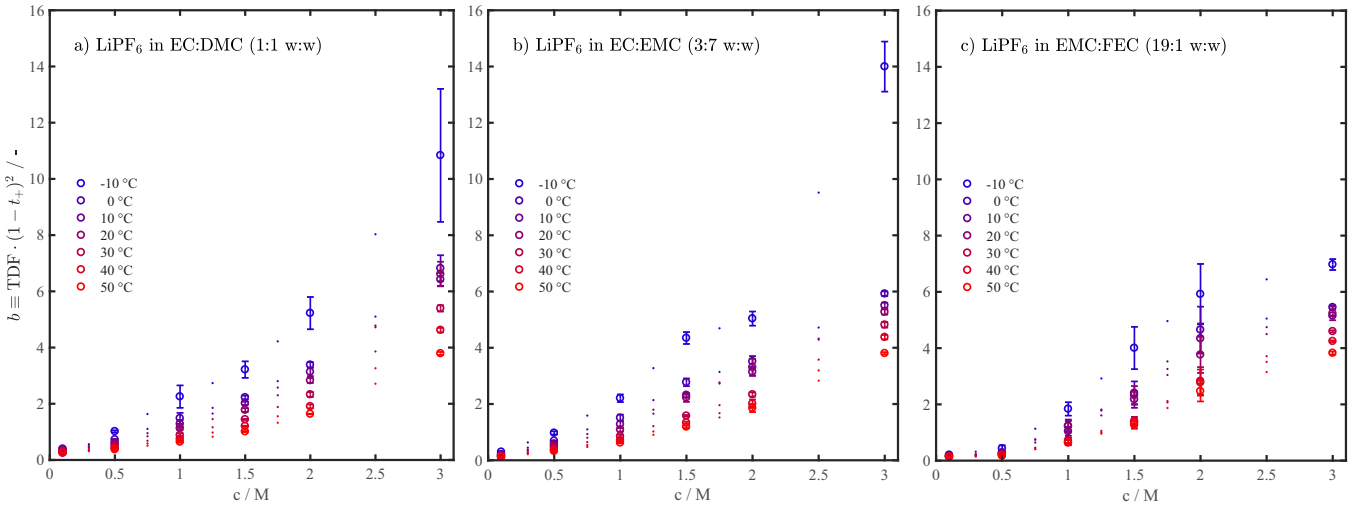

Figure 7. Transport factor $b(c_0) \equiv \mathrm{TDF}(c_0) \cdot (1 - t_+(c_0))^2$, vs. the mean molar $LiPF_6$ concentration and temperature (−10°C to +50°C; indicated by the color scheme in the figure) for $LiPF_6$ in: a) EC:DMC (1:1 w:w), b) EC:EMC (3:7 w:w), and, c) EMC:FEC (19:1 w:w). It is calculated with the above determined slope ($m_{\ln}$) of the long-term potential relaxation (exemplarily shown in Figure 5) and the potential $U(T_1)$ just after the current interrupt (exemplarily shown in Figure 6) by means of Eq. 11. Data points (circles) as well as linear interpolations to the mean concentrations from the concentration cell (dots at 0.3, 0.75, 1.25, 1.75, and 2.5 M $LiPF_6$) are shown. Errors are calculated as explained in the section 4. Error calculation and regression analysis in the supporting information with the individual b values x_i and their error based on the confidence interval of $U(T_1)$, as Δx_i, at least two cells were measured for each configuration and positive and negative current pulses are analyzed.

(1.06 measured at 0.75 M) and the linearly interpolated transport factor $b(0.75\ \mathrm{M}) = 0.59$ (from b values at 0.5 M of 0.42 and at 1.0 M of 0.75) to be $t_+(0.75\ \mathrm{M}) = 0.44$. Gaussian error propagation of Eqs. 13 and 14 is used for the calculation of the errors of transference number and thermodynamic factor using the individual errors of $a(c_0)$ and $b(c_0)$ as obtained from the data analysis. The reader is reminded that latter calculation omits the slight temperature inaccuracy of the pulse experiments at temperatures below 20°C, as this would only lead to an underestimation of the transport factor $b(c_0)$ by on the order of 1%.

In addition to reporting our measurement results, we aim at providing concentration and temperature dependent descriptions of the thermodynamic and transport parameters. Yet, because the temperature and concentration dependence of especially the thermodynamic factor and the transference number lack a solid theoretical foundation, empirical functions (here polynomials) are used to approximate the real temperature and concentration dependence. It is emphasized that the obtained functional descriptions only serve as an approximation and that better correlation with experimental data might be obtained for different types of base functions.

To give an overview, we first analyze all parameters using functions to describe the temperature and concentration dependence simultaneously. As this multi-temperature approach shows that the complex temperature and concentration dependence of the transference number and the thermodynamic factor make it challenging to obtain a comprehensive mathematical description, we subsequently analyze these two parameters on a per temperature basis.

***Concentration & temperature dependent description of* κ.—**Figure 8 summarizes the temperature and concentration dependencies of the ionic conductivity (a – c), the binary diffusion coefficient (d – f), the thermodynamic factor (g – i), and the transference number (j – l) for the three here examined electrolytes. In addition to experimental results and fitting curves to be discussed below, Figure 8 also shows parameter values reported in two literature studies. Although not exactly representing the EC:DMC (1:1 w:w) electrolyte used in this work, we include the evaluated fitting functions for the transport and thermodynamic parameters at −10°C and +50°C reported by Valøen and Reimers[8] for $LiPF_6$ in PC:EC:DMC (10:27:63 v:v:v) as a reference, since these data are widely used in battery models (see Figures 8a, 8d, 8g, and 8j). Here it should be noted, that Valøen and Reimers assumed that the transference number is concentration independent. Nyman et al. reported transport and thermodynamic parameters at +25°C for the EC:EMC (3:7 w:w)[23] based $LiPF_6$ electrolyte also used in our work, and we show their results as a reference in Figures 8b, 8e, 8h, and 8k as well.

The ionic conductivities determined from the conductivity cells increase with increasing temperature for all electrolytes and show a pronounced conductivity maximum. Highest conductivities are obtained between ∼0.75 M (at −10°C) and ∼1 M (at +50°C) in EC:DMC and EC:EMC, while the peak conductivities for the EC-free electrolyte are shifted to higher concentrations (∼1.25 M at −10°C to ∼1.6 M at +50°C). Most ionic conductivities lie in the range of ∼0.5 mS/cm (3.0 M $LiPF_6$ at −10°C) to ∼17 mS/cm (1.0 M $LiPF_6$ in EC:DMC (1:1 w:w) at +50°C). Generally, higher conductivities are obtained for the EC:DMC based electrolyte (Figure 8a), while the lowest conductivities are obtained with the EC-free electrolyte (Figure 8c). For 0.1 M $LiPF_6$ in EMC:FEC (19:1 w:w), the conductivities at all temperatures lie in the range from 0.05 mS/cm (−10°C) to 0.1 mS/cm (+50°C) and thus way below the conductivities found for the EC containing electrolytes at the same concentration (∼2–5 mS/cm, compare Figures 8a and 8b), which may be due to a higher degree of ion association. Also shown in Figures 8a–8c are the fits of the experimental data to an empirical relation proposed by Ehrl[27]

$$\kappa(c,T) = p_1 (1 + (T - p_2)) \cdot c \cdot \frac{\left(1 + p_3 \cdot \sqrt{c} + p_4 \cdot \left(1 + p_5 \cdot \exp\left(\frac{1000}{T}\right)\right) \cdot c\right)}{1 + c^4 \cdot \left(p_6 \cdot \exp\left(\frac{1000}{T}\right)\right)} \cdot \frac{\mathrm{mS}}{\mathrm{cm}} \quad [15]$$

with six fitting parameters p_i. Here, as well as in the subsequently given empirical fitting equations, the concentration c is used in units of molar concentrations (mol/L) and the temperature in units of Kelvin (K). While Eq. 15 is entirely empirical, it was chosen to fulfil two theoretical limits: i) for infinitely low concentrations $\kappa(c,T)$ approaches 0 (no negative values allowed)

$$\lim_{c \to \infty} \kappa(c,T) = 0 \quad [16]$$

and, ii) the Kohlrausch square root law is obtained in the small concentration limit[28]

$$\lim_{c \to 0} \kappa(c,T) = p_a \cdot c + p_b \cdot c^{\frac{3}{2}}. \quad [17]$$

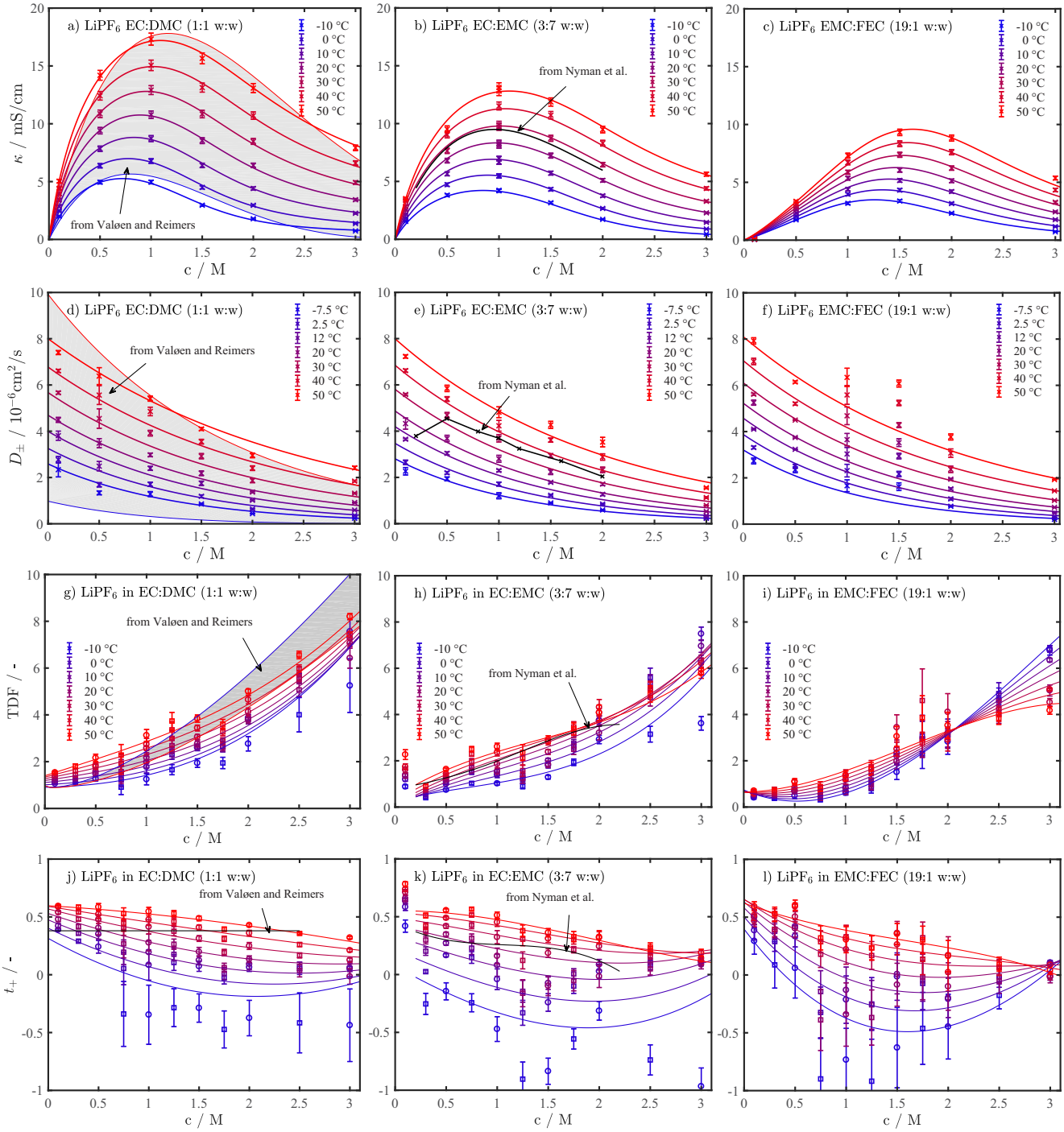

Figure 8. Ionic conductivity κ (a–c), binary diffusion coefficient $D_\pm$ (d–f), thermodynamic factor TDF (g–i), and transference number t_+ (j–l) between −10°C and +50°C (see legends for temperature scale placed in the plots in the left column) of 0.1–3.0 M $LiPF_6$ in EC:DMC (1:1 w:w), EC:EMC (3:7 w:w), and EMC:FEC (19:1 w:w). These property values (symbols) are determined as described in Figure 1 and in the Data Analysis section; numerical fitting (solid lines) is based on the empirical equations given by Eq. 15 (κ), Eq. 18 ($D_\pm$), Eq. 19 (TDF), and Eq. 20 (t_+), whereby the determined fitting parameters p_i and the goodness of fit values are given in Table II. Additionally depicted are property data reported in the literature: in the left column for $LiPF_6$ in PC:EC:DMC (10:27:63 v:v:v) by Valøen and Reimers[8] (gray shaded area with the blue line marking −10°C and the red line marking +50°C) and in the middle column for $LiPF_6$ in EC:EMC (3:7 w:w) at 25°C by Nyman et al.[23] (solid black line). Error bars for κ correspond to 3% to account for the error of the cell constant, cell filling, and fitting. Error bars for $D_\pm$ depict the standard deviation of the weighted mean as described in the Data Analysis and the section 4. Error calculation and regression analysis in the supporting information. Error bars for the TDF and for t_+ are calculated using Gaussian error propagation of Eq. 13 and Eq. 14, with the individual errors of a and b as described in the Data Analysis section.

Very good agreement of the fits can be found for all three solvent mixtures (R^2 values >0.995 for all solvents in Table II); the obtained fitting parameters are given in Table II, including their 95% confidence bounds. Conductivities reported for EC:DMC (1:1 w:w) generally agree well with the similar electrolyte composition reported by Valøen and Reimers (PC:EC:DMC 10:27:63 v:v:v), as shown for reference in Figure 8a (gray highlighted region with the same lower limit of −10°C and the same upper limit of +50°C).[8] In addition, we show the conductivities measured by Nyman et al. for EC:EMC (3:7 w:w) at 25°C as a black solid line in Figure 8b,[23] which are reasonably close

Table II. Fitting parameter p_i for the empirical approximations of the ionic conductivity (Eq. 15), the binary diffusion coefficient (Eq. 18), the thermodynamic factor (Eq. 19), and the transference number (Eq. 19) for 0.1–3.0 M $LiPF_6$ in EC:DMC (1:1 w:w), EC:EMC (3:7 w:w), and EMC:FEC (19:1 w:w) in the temperature range from −10°C to + 50°C. Also given here are the 90% confidence bounds and the goodness of fit values R^2 for the individual fits. The fitting curves are plotted in Figure 8.

Parameter		EC:DMC (1:1 w:w)		EC:EMC (3:7 w:w)		EMC:FEC (19:1 w:w)	
$\kappa(c,T)$	p_1	7.98E−01	(5%)	5.21E−01	(5%)	2.51E−02	(54%)
Eq. 15	p_2	2.28E+02	(1%)	2.28E+02	(1%)	1.75E+02	(22%)
	p_3	−1.22E+00	(4%)	−1.06E+00	(2%)	1.23E+00	(117%)
	p_4	5.09E−01	(10%)	3.53E−01	(8%)	2.05E−01	(329%)
	p_5	−4.00E−03	(13%)	−3.59E−03	(19%)	−8.81E−02	(323%)
	p_6	3.79E−03	(28%)	1.48E−03	(42%)	2.83E−03	(32%)
	R^2	0.999		0.997		0.995	
$D_\pm(c,T)$	p_1	1.47E+03	(75%)	1.01E+03	(87%)	5.86E+02	(118%)
Eq. 18	p_2	1.33E+00	(39%)	1.01E+00	(79%)	1.33E+00	(59%)
	p_3	−1.69E+03	(14%)	−1.56E+03	(17%)	−1.38E+03	(26%)
	p_4	−5.63E+02	(28%)	−4.87E+02	(50%)	−5.82E+02	(41%)
	R^2	0.989		0.978		0.969	
$TDF(c,T)$	p_1	−5.58E+00	(433%)	2.57E+01	(123%)	3.22E+00	(597%)
Eq. 19	p_2	7.17E+00	(237%)	−4.51E+01	(57%)	−1.01E+01	(151%)
	p_3	3.80E−02	(431%)	−1.77E−01	(122%)	−1.58E−02	(833%)
	p_4	1.91E+00	(61%)	1.94E+00	(99%)	6.12E+00	(18%)
	p_5	−6.65E−02	(173%)	2.95E−01	(60%)	2.96E−02	(350%)
	p_6	−5.08E−05	(545%)	3.08E−04	(120%)	2.42E−05	(927%)
	p_7	1.10E−01	(90%)	2.59E−01	(71%)	−2.22E−01	(46%)
	p_8	−6.10E−03	(65%)	−9.46E−03	(67%)	−1.57E−02	(22%)
	p_9	1.51E−04	(130%)	−4.54E−04	(67%)	6.30E−06	(2802%)
	R^2	0.981		0.943		0.979	
$t_+(c,T)$	p_1	−7.91E+00	(73%)	−1.28E+01	(94%)	−1.22E+01	(93%)
Eq. 20	p_2	2.45E−01	(1428%)	−6.12E+00	(128%)	−3.05E+00	(198%)
	p_3	5.28E−02	(74%)	8.21E−02	(99%)	8.38E−02	(91%)
	p_4	6.98E−01	(33%)	9.04E−01	(70%)	1.78E+00	(30%)
	p_5	−1.08E−02	(217%)	3.18E−02	(164%)	1.51E−03	(2629%)
	p_6	−8.21E−05	(80%)	−1.27E−04	(108%)	−1.37E−04	(95%)
	p_7	7.43E−04	(2542%)	1.75E−02	(303%)	−2.45E−02	(177%)
	p_8	−2.22E−03	(33%)	−3.12E−03	(61%)	−5.15E−03	(31%)
	p_9	3.07E−05	(129%)	−3.96E−05	(222%)	2.14E−05	(308%)
	R^2	0.930		0.823		0.808	

to our data at 30°C. Although not shown explicitly in Figure 8a, our measurement for 1.0 M $LiPF_6$ in EC:DMC (1:1 w:w) also agrees well with the value reported by Farkhondeh et al.[17] (11.9 mS/cm at 25°C vs. 10.8-12.9 mS/cm at 20–30°C in our study). To further validate our measurements, we compared the temperature dependence of the 1.0 M electrolyte conductivities for EC:DMC (1:1 w:w) and EC:EMC (3:7 w:w) with the specification sheet from BASF for their electrolytes of the same composition (tradenames LP30 and LP57), obtaining very good agreement (see Supporting Information Figure S2).

Concentration & temperature dependent description of $D_\pm$.— Figures 8d–8f depicts the concentration and temperature dependent binary diffusion coefficients we obtain from the analysis of the long-term potential relaxation after galvanostatic pulses for the three electrolyte solutions (see Figure 5 in the section Data Analysis and Ref. 5). The diffusion coefficients in Figure 8 are empirically fitted with

$$D_\pm(c,T) = p_1 \cdot \exp(p_2 \cdot c) \cdot \exp\left(\frac{p_3}{T}\right) \cdot \exp\left(\frac{p_4}{T} \cdot c\right) \cdot 10^{-6}\frac{\text{cm}^2}{\text{s}} \quad [18]$$

with four free fitting parameters p_1 to p_4. The first two terms in Eq. 18 are identical with the terms we had used previously to describe the concentration dependence of $D_\pm$ at constant temperature,[5] the third term was selected to be in accord with an Arrhenius type temperature dependence (i.e., $D_\pm \propto p_a \cdot \exp(\frac{p_b}{T})$), while the last concentration-temperature cross-term was required to satisfactorily fit all $D_\pm$ data. In contrast to the clearly different ionic conductivities, the diffusion coefficients of all three electrolytes are found to be almost identical at a given temperature, as may be illustrated for the lowest and highest $LiPF_6$ concentration: i) at 0.1 M $LiPF_6$, the diffusion coefficients range from $\approx 2.3-7.4 \cdot 10^{-6}$ cm^2/s for EC:DMC (1:1 w:w) and EC:EMC (3:7 w:w) as well as from $\approx 2.7-8.0 \cdot 10^{-6}$ cm^2/s for EMC:FEC (19:1 w:w), as the temperature increases from −7.5°C to +50°C, respectively; ii) at 3.0 M $LiPF_6$, $D_\pm$-values range from $\approx 0.2-2.4 \cdot 10^{-6}$ cm^2/s (EC:DMC (1:1 w:w)), $\approx 0.2-1.6 \cdot 10^{-6}$ cm^2/s (EC:EMC (3:7 w:w)), and $\approx 0.2-2.0 \cdot 10^{-6}$ cm^2/s (EMC:FEC (19:1 w:w)) for the same temperature increase (compare Figures 8d–8f). The observed decrease of the binary diffusion coefficient with increasing concentration is expected according to the Stokes-Einstein relation due to the concomitant increase in electrolyte viscosity.[28] The ionic conductivity as well as the binary diffusion coefficient directly depend on the ionic mobility and it therefore is surprising that very similar diffusion coefficients are obtained for the three different electrolyte solvent mixtures while the ionic conductivities show pronounced differences (compare Figures 8a–8f). A plausible explanation could be the extent of ion association which strongly affect the ionic conductivity but not the diffusivity, as discussed in the literature.[29,30] An increase of ion association (i.e., of contact ion-pair formation), which would lead to a decrease in conductivity, was reported to occur as the molar ratio of cyclic to linear alkyl carbonates decreases (for PC:DMC

mixtures[31] as well as for ED:DEC mixtures[32]). Thus, the observed decrease in conductivity as the concentration of the cyclic carbonate (EC or FEC) content in the solvent mixture is decreased from 50 wt% (EC:DMC) to 30 wt% (EC:EMC) and to 5 wt% (EMC:FEC) as shown in Figures 8a–8c is consistent with the expected increase of ion association.

In all cases, the chosen temperature and concentration dependent fit function for the diffusion coefficient (Eq. 18) represents the experimental data well, although a higher scatter of the data is observed compared to the above discussed ionic conductivity measurements. Both symmetric lithium coin cells filled with the 1.5 M $LiPF_6$ in EMC:FEC (19:1 w:w) yield somewhat higher diffusion coefficients than expected from the neighboring 1.0 and 2.0 M electrolytes (see Figure 8f). The scatter and the simultaneously small error bars, based on the statistical variation of repeat measurements (here 2 cells with 2 pulses each) indicate that a systematic error due to, e.g., cell building effects or separator inhomogeneities are not accounted for in our error analysis and that the data quality would profit from a higher number of repeat cells. Still, a reasonably good correlation of the experimental data with Eq. 18 can be obtained in all cases, yielding R^2 values of 0.97 and above (see Table II for R^2 values and fit parameters p_i). Reported diffusion coefficients in the literature[8,17,23] generally show similar values. As a first example, we compare the data by Valøen and Reimers[8] obtained in a similar electrolyte ($LiPF_6$ in PC:EC:DMC (10:27:63 v:v:v)), which are marked by the gray highlighted area in Figure 8d (upper light red line for +50°C and lower light blue line for −10°C). While the $D_\pm$ values are reasonably similar, their temperature and concentration dependence nevertheless is quite a bit stronger compared to the measurements in our study (see gray highlighted region in Figure 8d). This different behavior is most likely due to the fact that $D_\pm$ in the calculations by Valøen and Reimers is obtained from their initially determined transference number and thermodynamic factor (see Eq. 13 in Ref. 8); since the authors assume a concentration and temperature independent transference number, their diffusion coefficient will automatically incorporate these assumptions, which may not be correct. Because the diffusion coefficients determined in our study are obtained individually at a given concentration and temperature simply from the long-term potential relaxation after a galvanostatic pulse without needing any other transport properties (see scheme in Figure 1), we are quite confident that our values are correct and that the increased concentration dependence reported by Valøen and Reimers is due to their oversimplification of the concentration and temperature dependence of the transference number. A further comparison can be found for the 1.0 M $LiPF_6$ in EC:DMC (1:1 w:w) electrolyte, for which Farkhondeh et al.[17] report a binary diffusion coefficient of 2.7×10^{-6} cm^2/s at 25°C, which is reasonably close to our measurement (3.0×10^{-6} cm^2/s at 20°C and 3.9×10^{-6} cm^2/s at 30°C). For the $LiPF_6$ in EC:EMC (3:7 w:w) electrolyte at 25°C, Nyman et al.[23] report diffusion coefficients which are slightly higher than our diffusion coefficient in the same electrolyte obtained at 30°C (see black line in Figure 8e). This difference may be caused by errors in the used cell geometry parameters, e.g., the uncertainty in the porous medium tortuosity or the electrode distance in their setup.

Concentration & temperature dependent description of TDF.— Because the previously introduced direct measurement of the thermodynamic factor from ferrocene/ferrocenium redox potential measurements is not strictly valid, thermodynamic factors and transference numbers are calculated from the factors a and b (see Theory section as well as the scheme in Figure 1).[7,19] I.e., in contrast to the analysis of the ionic conductivity and the binary diffusion coefficient, single parameters cannot be obtained from a single measurement anymore, yielding an intrinsically higher uncertainty. Yet, we would like to emphasize that compared to the determination methods reported in the literature, no assumptions on the temperature and concentration dependence of either transference number or thermodynamic factor have to be made (like, e.g., a concentration and temperature independent transference number as made in Ref. 8), to that the obtained values of t_+ and TDF are explicit. In Figures 8g–8l, the data points based on the measured factor $a(c_0)$ from concentration cell experiments are plotted as squares and the data points based on the measured factor $b(c_0)$ from the pulse experiments are plotted as circles (i.e., analogous to Figure 4 and Figure 7, the reader is reminded that the transport factor $b(c_0)$ includes a small systematic error due to the temperature offset of the temperature chamber for the pulse experiments as described in the Experimental). The thermodynamic factors we obtain from the analysis of the temperature and concentration dependent concentration potentials and the analysis of the short-term potential relaxation after galvanostatic pulses in a symmetric Li-Li coin cell are depicted in Figures 8g–8i. We deliberately start discussing the TDF rather than the transference number, as it may be compared (at least partly) with theoretical considerations. By definition, the mean molar activity coefficient and the TDF ($\equiv 1 + \frac{d \ln f_\pm}{d \ln c}$) are 1 at infinite dilution and initially decrease with increasing concentration according to the Debye-Hückel theory,[24] thereby serving as a quality measure for the experimentally obtained data. It is emphasized that the calculation of the TDF according to Eq. 14 is unbiased in terms of a fixed reference value, so that we would expect a value of TDF = 1 at infinite dilution and an initial decrease of TDF with increasing temperature. As a matter of fact, the obtained TDF-values are close to 1 in the low-concentration limit (∼0.5 and ∼1.5 for EC:DMC (1:1 w:w) and EMC:FEC (19:1 w:w) at −10°C and at +50°C, respectively), and in the EMC:FEC electrolyte an initially small decrease of the TDF-values with increasing concentrations can be observed (see Figure 8i).

On the other hand, the TDF-values for $LiPF_6$ in EC:EMC (3:7 w:w) lie well above the theoretical low concentration limit (∼1–2.2 at 0.1 M, see Figure 8h), indicating that the measurements are erroneous, which we believe is due to a poor and unstable passivation of the metallic lithium electrodes. The reader is reminded that these data points are based on measured transport factors $b(c_0)$ from the short-term relaxation after a current pulse in symmetric Li-Li coin cells nominally containing 0.1 M $LiPF_6$. At such low salt concentrations, side reactions due to, e.g., the reformation of the SEI may alter the electrolyte composition and thus invalidate the application of concentration dependent analytical solutions such as Eq. 11 (see also discussion in section "Transference number via polarization cell and concentration cell experiments" in Ref. 6). The hypothesis of ongoing side reactions in these cells is further supported by analysis of the apparent separator tortuosity based on the high frequency impedance recorded of the symmetric cells prior to each pulse application:[1] if the electrolyte is stable versus the metallic lithium electrodes, the obtained separator tortuosity (a purely geometrical parameter) should be temperature and concentration invariant; on the other hand, if the electrolyte composition varies over the course of the experiments, the obtained apparent tortuosity values would vary. The analysis of the Nyquist plots recorded for all three electrolytes in the temperature range from +10°C to +50°C in symmetric Li-Li coin cells filled with the 0.1 M electrolytes yield tortuosities of 4.6 for EC:DMC (1:1 w:w), 5.2 for EMC:FEC (19:1 w:w), but 2.6 for EC:EMC (3:7 w:w). Thus, for the first two cases the apparent tortuosity is essentially identical to the independently obtained tortuosity value (4.8 ± 0.4, see Coin Cells in the Experimental section), but the much smaller apparent tortuosity obtained for the EC:EMC based electrolyte with 0.1 M $LiPF_6$ clearly shows the electrolyte's instability toward metallic lithium, leading to a change in electrolyte conductivity. Therefore, we could not include the data obtained for 0.1 M $LiPF_6$ in EC:EMC (3:7 w:w) in our analysis of the thermodynamic factor and the transference number; the data is only shown for the interested reader, as they serve to demonstrate a critical quality check for the experiments at low concentrations. In addition, the −10°C coin cell experiments of the EC:DMC based electrolytes below 1 M $LiPF_6$ were inconclusive (apparent tortuosities before pulse application >10) and are discarded in the following analysis of TDF and t_+. A possible explanation for the EC:DMC electrolyte could be the comparably high freezing temperature of the solvent mixture, which is ∼5°C for the used solvent ratio in this study and which may be lowered insufficiently with the 0.1 M and 0.5 M salt concentrations.[33] The largest errors of the TDF are observed for ∼1.5–2 M $LiPF_6$ in EMC:FEC (19:1 w:w, compare Figure 8i) and coincide with the in-

creased errors in the diffusion coefficients (see Figure 8f), which suggests an experimental artefact in the corresponding coin cells.

Up to 2.0 M salt concentrations, the TDF-values increase with temperature for all solvents (see Figures 8g–8i). At salt concentrations above 2.0 M, the temperature dependence inverts, which is partially visible with EC:DMC (1:1 w:w) in Figure 8g and EC:EMC (3:7 w:w) in Figure 8h, and which can clearly be observed for EMC:FEC (19:1 w:w) in Figure 8i. This clear inversion might be related to the amount of strongly solvating EC (or FEC) molecules, which decreases from 50 wt% (EC:DMC) to 30 wt% (EC:EMC) and to 5 wt% (EMC:FEC). Especially at high salt concentrations, the number of free, i.e., unsolvated EC (or FEC) molecules will decrease and might drastically change the ion activity; however, a physical interpretation of this inversion is clearly beyond the scope of this work. Instead we focus on the discussion of the obtained fits and comparable literature reports.

As mentioned before, no theoretical foundation for the temperature and concentration dependence of the thermodynamic factor in non-aqueous electrolytes is known. Therefore, we use simple polynomial functions to approximate our measured TDF-values. Specifically we use a polynomial of the form

$$\mathrm{TDF}\,(c,T) = p_1 + p_2\cdot c + p_3\cdot T + p_4\cdot c^2 + p_5\cdot c\cdot T + p_6\cdot T^2 + p_7\cdot c^3 + p_8\cdot c^2\cdot T + p_9\cdot c\cdot T^2 \quad [19]$$

with nine free fitting parameters p_i (see fitting results in Table II). As before, the temperature is used in units of Kelvin and the concentration in units of mol/L (M). The concentration dependence in Eq. 19 is described by a 3rd order polynomial, the temperature dependence by a 2nd order polynomial; higher order polynomials did not improve the quality of the fit. Reasonable agreement with experimentally obtained TDFs is found for EC:DMC (1:1 w:w, Figure 8g) and EMC:FEC (19:1 w:w, Figure 8i) as also indicated by the R^2 values of 0.99 in Table II. Unfortunately the EC:EMC based electrolyte (see Figure 8h) shows the highest experimental scatter and thus a high quality correlation with concentration and temperature cannot be obtained (R^2 value of 0.89 in Table II). The reader is reminded that the temperature and concentration dependent functional descriptions as well as their fit parameters (as given in Table II) only serve as an approximation and are provided as simple correlations for use in temperature dependent battery models, which, however, should be considered approximate in nature; when only modeling at single temperatures, the subsequently shown individually fitted correlations vs. concentration are likely more reliable.

Larger experimental uncertainties make it difficult to unambiguously compare our results with the literature. Within experimental variation, the TDF-values for 0.35 M to 2 M $LiPF_6$ in EC:EMC (3:7 w:w) agree reasonably well with the literature (see black line in Figure 8h, depicting the data by Nyman et al.[23] in the same electrolyte at 25°C). The thermodynamic factor reported by Farkhondeh et al. for 1 M $LiPF_6$ in EC:DMC (1:1 w:w) of 2.3 at 25°C is in good agreement with our results (2.2 at 20°C and 2.6 at 30°C).[17] Comparison of the TDFs of $LiPF_6$ in EC:DMC (1:1 w:w) with the widely used data by Valøen and Reimers[8] for a similar electrolyte ($LiPF_6$ in PC:EC:DMC (10:27:63 v:v:v), see gray region in Figure 8g) differs in two aspects: i) their TDF-values start at 1 for all temperatures, which, however, was implicitly assumed in their analysis; ii) more importantly, their temperature dependence of the TDF is inversed compared to our data (see blue upper boundary of gray highlighted region in Figure 8g, corresponding to −10°C, and red lower boundary corresponding to +50°C). The increase of the TDF with increasing temperature found in our study was also reported for $LiPF_6$ in EC:DEC (1:1 w:w) by Lundgren et al.[9] Similar to our previous argument with regards to the concentration and temperature dependence of the diffusion coefficient, we are confident that the opposite temperature dependence of the TDF reported by Valøen and Reimers[8] directly follows from their concentration and temperature invariant transference number (as in their case TDF is calculated from $v(c,T) = (1-t_+)\cdot \mathrm{TDF}$ under the assumption that $t_+ = \text{const.}$, compare Eq. 3 in Ref. 8).

Concentration & temperature dependent description of t_+.—At last we discuss the concentration and temperature dependence of the transference numbers, shown for the here examined electrolytes in Figures 8j–8l; while the transport factor $b(c_0)$ includes a small systematic error due to the temperature offset for the pulse experiments, this effect is minor and has been ignored here (see the relevant discussion in the Experimental section). As before, the transference numbers for 0.1 M $LiPF_6$ in EC:EMC (3:7 w:w) are only shown for the sake of completeness, but are omitted in the analysis due to the above discussed electrolyte instability with metallic lithium. To fit the temperature and concentration dependence of t_+, we used the same arbitrarily chosen polynomial as for the TDF (fitting parameters p_i are listed in Table II):

$$t_+\,(c,T) = p_1 + p_2\cdot c + p_3\cdot T + p_4\cdot c^2 + p_5\cdot c\cdot T + p_6\cdot T^2 + p_7\cdot c^3 + p_8\cdot c^2\cdot T + p_9\cdot c\cdot T^2 \quad [20]$$

The found transference numbers decrease with decreasing temperature and increasing concentration. The transference number varies between 0.38 (0°C) and 0.59 (+50°C) for 0.1 M $LiPF_6$ in EC:DMC (1:1 w:w), −0.25 (0°C) and 0.51 (+50°C) for 0.35 M $LiPF_6$ in EC:EMC (3:7 w:w), and 0.29 (0°C) and 0.59 (+50°C) for 0.1 M $LiPF_6$ in EMC:FEC (19:1 w:w). For typically used 1 M $LiPF_6$ concentrations at 20°C, we find transference numbers of 0.27 (the fit suggests 0.28, see Table II and Figure 8j) for EC:DMC (1:1 w:w), 0.16 (the fit suggests 0.22, see Table II and Figure 8k) for EC:EMC (3:7 w:w), and −0.34 (outlier with large error; the fit suggests 0.11, see Table II and Figure 8l) for EMC:FEC (19:1 w:w). Our low temperature measurements, especially at −10°C show large errors at all concentrations as well as negative values (see blue circles and squares in Figures 8j–8l). Negative transference numbers were previously motivated in the literature with ion triplet formation.[34] It is noted that ion triplets are beyond the scope of the herein used binary electrolyte model, but the presence of more than two charge carrying entities could be an explanation for the observed negative values of the transference number in this analysis. Yet, as will be visible more clearly in the single temperature fits in Figure 10, our measurements from 0°C to +50°C mostly lie (within the error) inside the theoretically defined range for transference numbers (0 to 1), and we suspect that the statistical errors of the −10°C data underestimate the experimental uncertainty. Qualitatively this is in accord with the analysis of the temperature and concentration dependent transport factor $b(c_0)$ at −10°C, which shows a clear offset from all the other temperatures (see Figure 7). At 3 M salt concentrations the transference numbers are close to 0 for the EC:EMC (0.09 to 0.20, outlier at −10°C at ∼−1, compare Figure 8k) and the EMC:FEC electrolyte (−0.02 to 0.11, compare Figure 8l). When EC:DMC is used as a solvent the transference number remains surprisingly steady and values of 0.13 and 0.32 are measured for 3 M $LiPF_6$ at 30°C and 50°C respectively. Within experimental error, the transference number reported by Nyman et al.[23] at 25°C agrees well with our measurements (black line lies between our 20°C and 30°C values in Figure 8k). The transference numbers found for 1 M $LiPF_6$ in EC:DMC (1:1 w:w, compare Figure 8j) at 20°C (0.27) and 30°C (0.41) are slightly below the value reported by Farkhondeh et al.[17] for the same electrolyte at 25°C (0.42). Due to the assumption of a concentration and temperature invariant transference number, the value of Valøen and Reimers completely disagrees with our results, which is unlikely to be solely caused by the different solvent composition.[8] In addition to the above discussed transference number data, there are two more recent reports on the concentration and temperature dependence of t_+ for $LiPF_6$ in EC:DMC (1:1 w:w) by Krachkovskiy et al.[35] as well as in ED:DEC (1:1 w:w) by Feng et al.,[29] which are based on self-diffusion coefficients from NMR experiments. While Krachkovskiy et al.[34,35] report a slight decrease of t_+ with increasing $LiPF_6$ concentration at 30°C (from ∼0.34 to at 0.2 M to ∼0.31 at 2 M), Feng et al. report no clear trend of t_+ with $LiPF_6$ concentration at room temperature (up to 1.6 M, t_+ varies irregularly between ∼0.25 and ∼0.3).[35] Krachkovskiy et al. also reported that t_+ for 1 M $LiPF_6$ in EC:DMC (1:1 w:w) decreases with increasing temperature (from

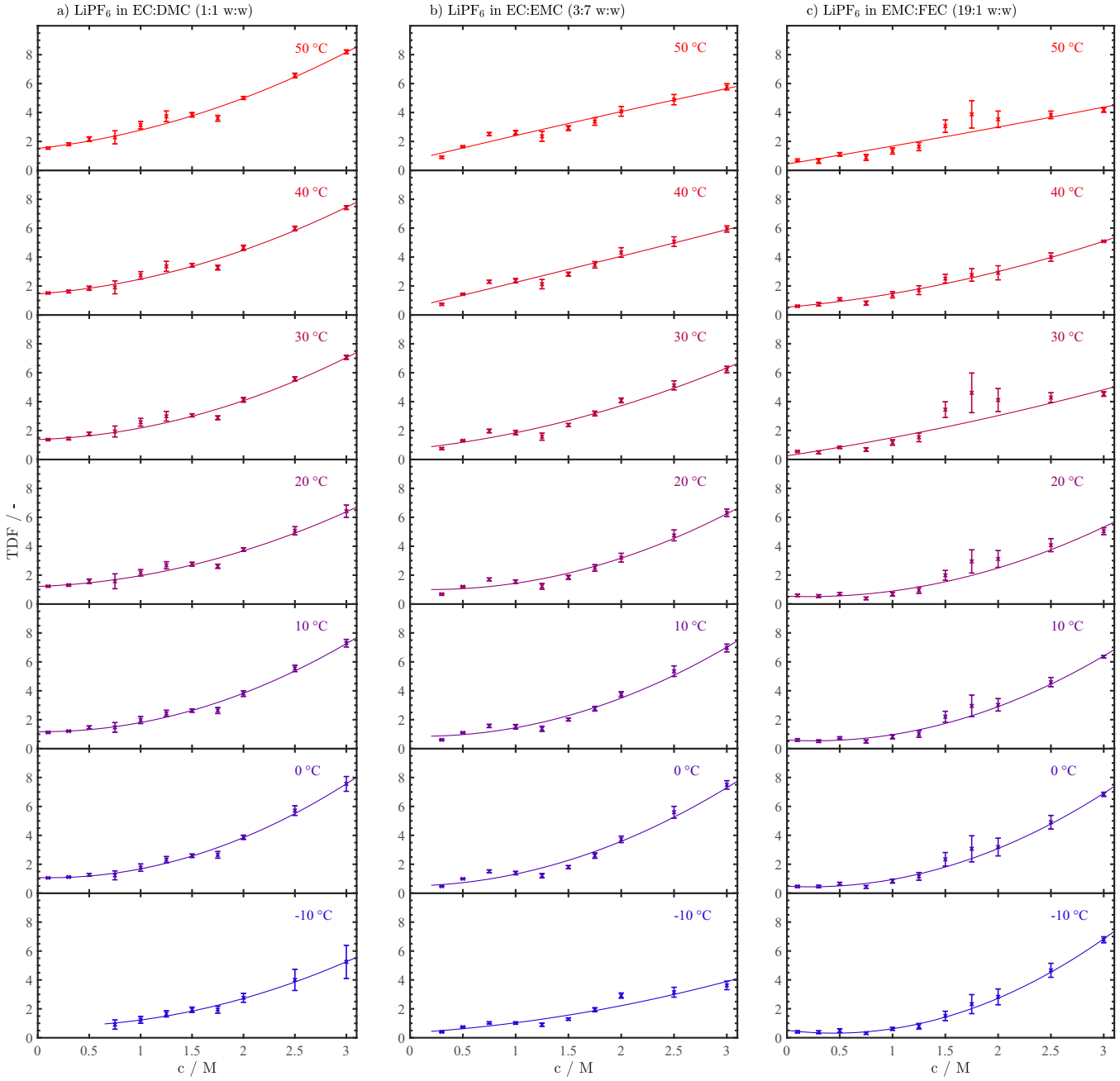

Figure 9. Thermodynamic factors for each temperature (−10°C to +50°C; see legends in the figure) of 0.1–3.0 M $LiPF_6$ in different solvents (same data as in Figures 8g–8i, but fitted individually): a) EC:DMC (1:1 w:w), b) EC:EMC (3:7 w:w), and, c) EMC:FEC (19:1 w:w). The thermodynamic factors are calculated from the transport factors a (Figure 4) and b (Figure 7) according to Eq. 14 (see Figure 1) and are approximated (solid lines) with the functional description given in Eq. 21 (the fitting parameters p_i and the goodness of fit values are given in Table III). Error bars are calculated using Gaussian error propagation of Eq. 14 with the individual errors of a and b as described in the Data Analysis and section 4. Error calculation and regression analysis in the supporting information.

∼0.35 at 5°C to ∼0.32 at 35 C),[35] opposite to our observations (see Figures 8j–8l).

Quite clearly, even for the very few available literature data on the concentration and temperature dependence of t_+ in $LiPF_6$ based electrolytes, there is no consistency in the literature. Our data show that t_+ in all of the three investigated solvent mixtures (Figures 8j–8l) decreases significantly with increasing salt concentration and with decreasing temperature, reaching negative values as the temperature goes below +10°C. A plausible explanation for negative t_+ values is the formation of triplet ions (i.e., $Li(PF_6)_2^-$) at low temperatures, a hypothesis which had been posed previously for a polymer electrolyte.[34] The very low or even negative transference numbers at (sub-)zero temperatures may be the explanation for the observed lithium plating at the separator/graphite interface during low-temperature charging of lithium ion batteries even at very low C-rates (e.g., at C/5 at −20°C[36,37]), because concentration gradients will form faster when the migration currents are negligible.[36,38,39]

The decrease of t_+ with increasing salt concentration may be explained with the two different Li^+ ion transport mechanisms discussed in the literature:[40] carrier-based transport (i.e., movement of the Li^+ ion with its solvation shell) and jump-diffusion-based transport (i.e., jumping of the Li^+ ion from one solvation shell configuration to another). Considering that the number of solvent molecules in the primary solvation shell around the Li^+ ion in linear/cyclic carbonate solvent mixtures is estimated to be between ∼3–5,[31,40] substantial complexation of all solvent molecules would be expected to occur at

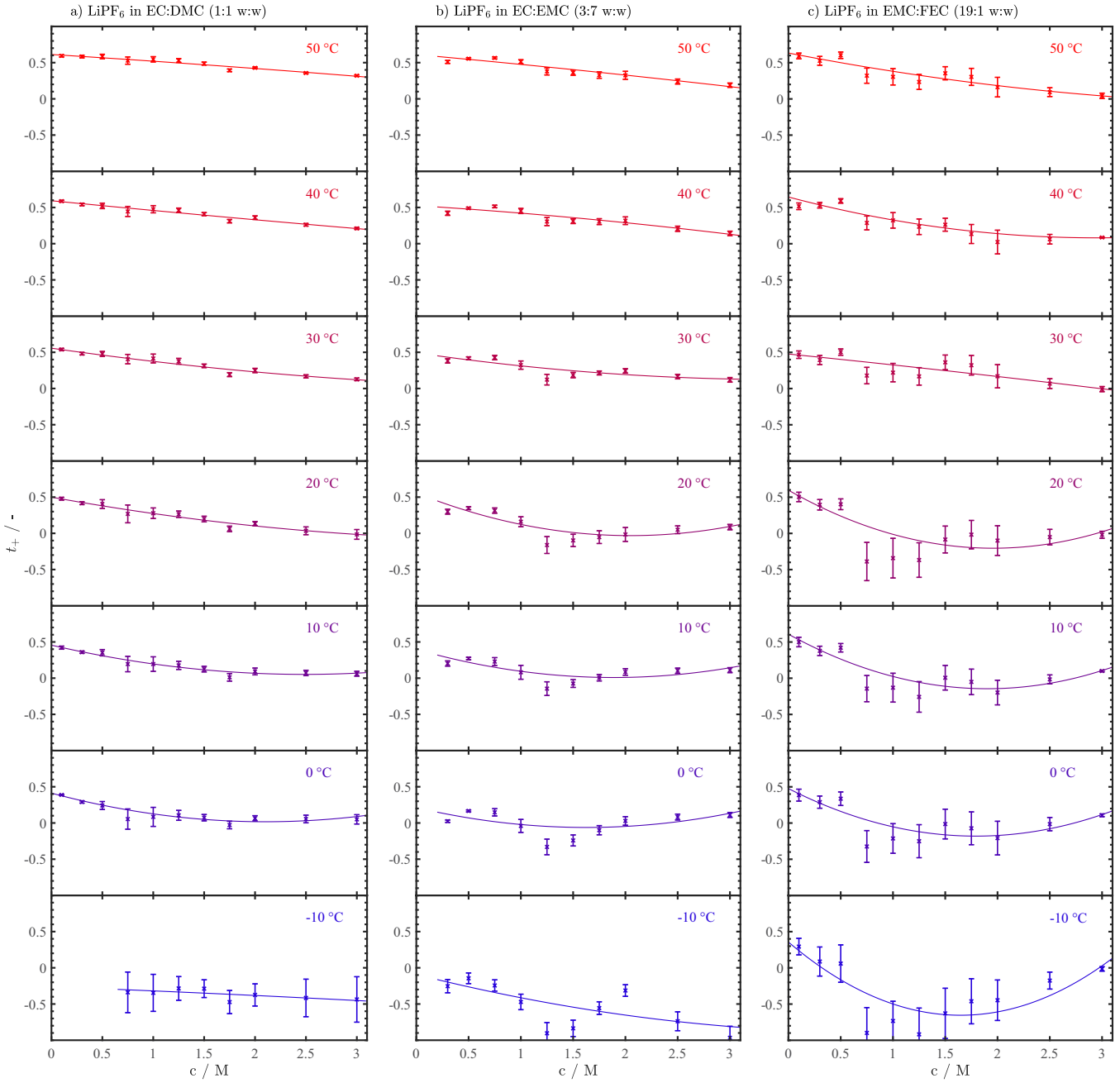

Figure 10. Individual transference numbers for each temperature (−10°C to +50°C; see legends in the figure) of 0.1–3.0 M $LiPF_6$ in different solvents (same data as in Figures 8j–8l, but fitted individually): a) EC:DMC (1:1 w:w), b) EC:EMC (3:7 w:w), and, c) EMC:FEC (19:1 w:w). The transference numbers are calculated from the transport factors a (Figure 4) and b (Figure 7) according to Eq. 13 (see Figure 1) and are approximated (solid lines) with the functional description given in Eq. 22 (the fitting parameters p_i and the goodness of fit values given in Table III). Error bars are calculated using Gaussian error propagation of Eq. 13 with the individual errors of a and b as described in the Data Analysis and section 4. Error calculation and regression analysis in the supporting information.

∼5 solvent molecules per Li^+, which would correspond to salt concentrations of ∼3 M for all three electrolytes in this study (calculated from the molecular weight of the solvents molecules and the electrolyte densities given in Figure S1 and Table S1). We conclude that it is quite plausible that a gradual retardation of carrier-based Li^+ ion transport at high concentrations and low temperatures might be responsible for the here observed concomitant decrease of t_+, due to an increasing fraction of the linear/cyclic carbonate solvents forming an immobilized framework through which the lithium ion with its solvation shell has to move. Although the probability for jump-diffusion-based transport may increase for increasing temperatures and Li^+ ion concentrations its contribution likely remains at a lower absolute level compared to the carrier-based transport. Such a dominance of the carrier-based Li^+ transport, together with the similar complexations of the lithium ions from the different solvent molecules, may also serve as a qualitative explanation for the similarity of the observed transference numbers.

Concentration dependent analysis of TDF and t_+ at fixed temperatures.—While in the previous section comprehensive functional descriptions for the temperature and the concentration dependence of the ionic and thermodynamic parameters were presented, in this section we are investigating the concentration dependences of the thermodynamic factor and the transference number for each temperature individually. Because a detailed analysis as well as the comparison with the literature was already presented in the above discussion of the multi-temperature fitting, we mainly show single

Table III. Fitting parameter p_i for the empirical approximations of the thermodynamic factor (Eq. 21) and the transference number (Eq. 22) for 0.1–3.0 M $LiPF_6$ in EC:DMC (1:1 w:w), EC:EMC (3:7 w:w), and EMC:FEC (19:1 w:w), determined individually for each temperature (−10°C to + 50°C). Also given here are their 90% confidence bounds and the goodness of fit values R^2. Fits for the thermodynamic factor and the transference number are graphically depicted for each temperature in Figure 9 and Figure 10, respectively.

Fitting Function			EC:DMC (1:1 w:w)		EC:EMC (3:7 w:w)		EMC:FEC (19:1 w:w)	
TDF(c, T)	−10°C	p_1	5.25E−01	(67%)	2.45E−01	(124%)	1.00E+00	(9%)
Eq. 21		p_2	−8.64E−02	(1408%)	4.49E−01	(193%)	−8.93E−01	(30%)
		p_3	7.93E−01	(124%)	3.41E−01	(144%)	5.16E−01	(27%)
		R^2	0.974		0.910		0.997	
	0°C	p_1	7.79E−01	(18%)	7.23E−01	(58%)	8.37E−01	(19%)
		p_2	−1.76E−01	(193%)	9.80E−02	(1135%)	−3.70E−01	(130%)
		p_3	1.08E+00	(10%)	5.00E−01	(90%)	4.79E−01	(48%)
		R^2	0.991		0.951		0.992	
	10°C	p_1	7.00E−01	(23%)	7.36E−01	(43%)	7.83E−01	(21%)
		p_2	−7.02E−02	(605%)	−1.55E−01	(587%)	−4.13E−01	(127%)
		p_3	1.17E+00	(16%)	8.63E−01	(56%)	5.93E−01	(45%)
		R^2	0.989		0.970		0.992	
	20°C	p_1	4.88E−01	(42%)	6.65E−01	(53%)	6.18E−01	(40%)
		p_2	2.56E−01	(202%)	−2.57E−01	(407%)	−2.60E−01	(284%)
		p_3	1.22E+00	(19%)	1.03E+00	(56%)	5.40E−01	(69%)
		R^2	0.976		0.952		0.957	
	30°C	p_1	5.44E−01	(35%)	3.70E−01	(88%)	1.33E−01	(281%)
		p_2	2.58E−01	(210%)	7.60E−01	(129%)	1.13E+00	(101%)
		p_3	1.38E+00	(20%)	7.17E−01	(78%)	2.48E−01	(207%)
		R^2	0.984		0.963		0.918	
	40°C	p_1	4.85E−01	(37%)	1.85E−02	(1735%)	2.90E−01	(44%)
		p_2	5.43E−01	(95%)	1.75E+00	(56%)	6.54E−01	(64%)
		p_3	1.45E+00	(18%)	4.80E−01	(114%)	5.28E−01	(39%)
		R^2	0.988		0.963		0.994	
	50°C	p_1	4.76E−01	(41%)	−3.29E−02	(1002%)	3.27E−02	(871%)
		p_2	7.89E−01	(71%)	1.76E+00	(58%)	1.21E+00	(72%)
		p_3	1.52E+00	(20%)	6.75E−01	(84%)	4.30E−01	(99%)
		R^2	0.989		0.955		0.937	
$t_+(c, T)$	−10°C	p_1	−3.23E−03	(3507%)	4.10E−02	(556%)	3.73E−01	(39%)
Eq. 22		p_2	−5.36E−02	(797%)	−3.63E−01	(197%)	−1.23E+00	(40%)
		p_3	−2.62E−01	(142%)	−9.17E−02	(511%)	3.56E−01	(84%)
		R^2	0.340		0.477		0.741	
	0°C	p_1	8.94E−02	(35%)	1.04E−01	(114%)	2.04E−01	(46%)
		p_2	−3.76E−01	(22%)	−3.38E−01	(111%)	−7.32E−01	(44%)
		p_3	4.12E−01	(9%)	2.13E−01	(95%)	4.76E−01	(38%)
		R^2	0.954		0.293		0.704	
	10°C	p_1	6.53E−02	(36%)	1.09E−01	(71%)	2.08E−01	(40%)
		p_2	−3.25E−01	(21%)	−4.12E−01	(61%)	−7.92E−01	(36%)
		p_3	4.56E−01	(8%)	3.98E−01	(40%)	6.08E−01	(26%)
		R^2	0.965		0.632		0.812	
	20°C	p_1	2.73E−02	(105%)	1.40E−01	(64%)	2.09E−01	(62%)
		p_2	−2.53E−01	(31%)	−5.74E−01	(51%)	−8.18E−01	(50%)
		p_3	5.00E−01	(8%)	5.57E−01	(31%)	5.96E−01	(37%)
		R^2	0.964		0.768		0.722	
	30°C	p_1	1.84E−02	(116%)	2.97E−02	(185%)	−4.75E−03	(1448%)
		p_2	−2.00E−01	(33%)	−2.10E−01	(85%)	−1.46E−01	(152%)
		p_3	5.57E−01	(7%)	4.92E−01	(24%)	4.77E−01	(26%)
		R^2	0.968		0.802		0.813	
	40°C	p_1	3.05E−03	(579%)	−1.39E−02	(370%)	6.49E−02	(86%)
		p_2	−1.37E−01	(40%)	−9.01E−02	(187%)	−3.83E−01	(50%)
		p_3	5.93E−01	(6%)	5.26E−01	(20%)	6.46E−01	(17%)
		R^2	0.971		0.864		0.923	
	50°C	p_1	−3.82E−03	(436%)	−5.87E−03	(791%)	2.77E−02	(187%)
		p_2	−8.89E−02	(59%)	−1.30E−01	(116%)	−2.80E−01	(59%)
		p_3	6.13E−01	(6%)	6.12E−01	(15%)	6.34E−01	(15%)
		R^2	0.958		0.906		0.915	

temperature fits for the benefit of the reader and only discuss the parameters concentration behavior briefly. As shown in Figures 8g–8i for the thermodynamic factor and in Figures 8j–8l for the transference number, experimental errors, the complex temperature behavior (see, e.g., Figure 8i), and the lack of a theoretical basis for the functional descriptions (Eqs. 19 and 20) make the simultaneous interpretation of the concentration *and* temperature dependence challenging. Although these general approximations might serve as a coarse approximation to the experimental results, experimentally found concentration dependencies are represented more reliably on a per temperature basis. Thus, we approximate in the following the experimentally obtained values for the thermodynamic factor and the transference number individually for each measurement temperature (−10°C to +50°C) using second order polynomials

$$\mathrm{TDF}\,(c) = p_1 \cdot c^2 + p_2 \cdot c + p_3 \quad [21]$$

$$t_+\,(c) = p_1 \cdot c^2 + p_2 \cdot c + p_3 \quad [22]$$

with three free fitting parameters p_i each, whereby concentrations are again given in units of mol/L (M). The individually shown values for each temperature (see separate panels in Figure 9 and Figure 10) and their fitting curves are shown in the figures, while the fitting parameters, their variation based on a 90% confidence interval, and the goodness of fit values are given in Table III. We believe that Figure 9 and Figure 10 allow for a more distinct judgement of the individual concentration dependencies compared to the depiction in Figure 8.

Thermodynamic factors for $LiPF_6$ in EC:DMC (1:1 w:w, Figure 9a), EC:EMC (3:7 w:w, Figure 9b), and EMC:FEC (19:1 w:w, Figure 9c) can be well approximated by their polynomial fit functions as judged by eye. However, the mathematically objective goodness of fit values are only above 0.94 for the EC:DMC and the EMC:FEC based electrolytes, while an inferior correlation ($R^2 > 0.81$) is found with the EC:EMC solvent system, in accord with the above discussion of generally larger errors for this electrolyte. Although the individual depiction of the concentration dependent transference numbers in Figure 10 make it much easier to follow its concentration dependence compared to Figure 8, the characteristic trends persist. From Figure 10, the very good correlation of the transference numbers with the selected second order polynomials for the EC:DMC based electrolyte can be observed clearly (Figure 10a). Starting from the linear behavior at 50°C (uppermost panel in Figure 10a), the observed trend converges to 0 at high concentrations and for lower temperatures. Only the −10°C measurements show negative transference numbers for all electrolytes (see Figure 10, panels for −10°C). Because these measurements are based on potentials measured in the pouch concentration cells as well symmetric lithium coin cells, an experimental artefact due to the cell setup seems unlikely. We rather think that the observed sudden change (also visible for transport factors a and b in Figure 4 and Figure 7) has to be related to the electrolyte, which possibly restructures when the temperature approaches the electrolyte freezing temperatures (we note that we assured in a separate experiment that none of the electrolyte solutions froze at −10°C as judged by eye). In summary we showed a reasonable description of the transference number for the EC:DMC solvent mixture and for temperatures above +20°C for the EC:EMC and EMC:FEC cases. Although thermodynamic factor and transference number are both based on the same transport factors a and b, the transference number as calculated from Eq. 13 is more sensitive toward errors (see generally larger errors for transference number in Figure 10 compared to thermodynamic factor in Figure 9). In conclusion a higher number of repeat measurements and an improved, less noise sensitive setup for the measurement of concentration potentials might enhance the experimental data quality and thus allows for a more rigorous analysis than the herein presented qualitative trends.

Conclusions

In this study we apply established methods for the determination of ionic conductivities and binary diffusion coefficients to $LiPF_6$ solutions in EC:DMC (1:1 w:w), EC:EMC (3:7 w:w) and EMC:FEC (19:1 w:w), covering a concentration range from 0.1 M to 3 M and a temperature range from −10°C to +50°C. Additionally we introduce a novel analysis scheme to quantify transference numbers and thermodynamic factors for the same electrolyte solutions and measurement conditions (concentration and temperature), based on the analysis of concentration cell potentials and the short-term potential relaxation after galvanostatic pulses in symmetric lithium coin cells. We carefully describe the analysis procedure and the calculation of the final transport properties and their errors for exemplary data and thereby ensure that the presented methodology can be utilized for the characterization of novel electrolytes with low effort. Our stringent comparison with the (scarcely) available literature shows good the qualitative agreement with the data by Nyman et al.,[23] the strong decrease of the Li^+ ion transference number with increasing $LiPF_6$ concentration and decreasing temperature obtained in our measurements is in contrast to the widely adopted publication by Valøen and Reimers,[8] who had assumed a temperature and concentration independent transference number. For the use in predictive battery models, we provide temperature and concentration dependent approximations to empirical and semi-empirical functions, and report the obtained fit parameters as well as their errors in tabulated form.

Acknowledgment

We gratefully acknowledges the funding by the Bavarian Ministry of Economic Affairs and Media, Energy, and Technology for its financial support under the auspices of the EEBatt project and the BMBF (Federal Ministry of Education and Research, Germany) for its financial support within the ExZellTUM II project (grant number 03XP0081). We thank rhd Instruments for providing the conductivity measurement cell, Jörg Schuster for encouraging us to extend our measurements to 3 M concentrations, Askin Eldiven for electrolyte density measurements, Tobias Greese from the ZAE Bayern for plasma treating the Nitto separators, Anna Freiberg for fruitful discussions on the experimental setup and Andreas Ehrl for our previous, tireless teamwork, which was key for the present study. Special thanks also goes to Jürgen Höhn (glass compartment cells), Korbinian Schmidt, and Simon Erhard (Peltier-element controlled temperature chamber) as well as Stefanie Neuner (16 channel multiplexer) for their valuable support and the manufacturing of custom-made equipment, although finally not applicable for the current work. We also thank Nathan Craig for motivating us to rethink the activity coefficient determination and Davide Menga, Hany El-Sayed, and Robert Morasch for valuable discussions and support with troubleshooting the ferrocene cell setup. Thanks also go to Bharatkumar Suthar for helpful comments on the manuscript.

List of Symbols

Symbol	Name	Unit
a	transport factor	-
$A_{\mathrm{El.}}$	electrode area	cm^2
b	transport factor	-
c	concentration	mol/L
$D^*_{\pm,\mathrm{eff}}$	effective binary diffusion coefficient	cm^2/s
$D_\pm$	binary diffusion coefficient	cm^2/s
$f_\pm$	mean molar activity coefficient	-
F	Faraday constant	As/mol
I_P	pulse current	µA
k_c	conductivity cell constant	1/cm
i	current density	
$l_{\mathrm{Sep.}}$	separator thickness	µm
$m_{\ln}$	slope of exp. pot. relaxation	1/s
n	number of measurements	-
p_i	fit parameter	-
Q	constant phase element (CPE)	$mF{\cdot}s^{\alpha-1}$
R	gas constant	J/(mol K)
R_{HFR}	high frequency resistance in cond. cell	Ohm

R_{CC}	resistance of conc. cell	Ohm
t	time	s
t_+	transference number of lithium ion	-
T	temperature	K
T_I	current interrupt time	s
TDF	thermodynamic factor	-
U_{CC}	conc. cell potential	V
U_{Offset}	long term potential offset	V
ν_+, ν_-	stoichiometric coefficients of the salt	-
w_i	weighing factor	various
$\bar{x}$	weighted mean	various
x_i	value	various
z_+, z_-	ion charge (>0 for cations, <0 for anions)	-

Greek

α	constant phase exponent	-
ε	porosity of porous medium	-
$\varepsilon_{Sep.}$	separator porosity	-
κ	electrolyte conductivity	mS/cm
Φ	vol. intr. phase average of the el. pot. w.r.t. a Li ref. el.	V
τ^*	artificial time	-
$\Delta\bar{x}$	error of weighted mean	various

ORCID

Johannes Landesfeind https://orcid.org/0000-0003-0333-2185

References

1. J. Landesfeind, J. Hattendorff, A. Ehrl, W. A. Wall, and H. A. Gasteiger, *J. Electrochem. Soc.*, **163**, A1373 (2016).
2. J. Landesfeind, M. Ebner, A. Eldiven, V. Wood, and H. A. Gasteiger, *J. Electrochem. Soc.*, **165**, A469 (2018).
3. J. Landesfeind, A. Eldiven, and H. A. Gasteiger, *J. Electrochem. Soc.*, **165**, A1122 (2018).
4. J. Newman and K. Thomas-Alyea, *Electrochemical Systems*, 3rd ed., Wiley Interscience, Hoboken, (2004).
5. A. Ehrl, J. Landesfeind, W. A. Wall, and H. A. Gasteiger, *J. Electrochem. Soc.*, **164**, A826 (2017).
6. A. Ehrl, J. Landesfeind, W. A. Wall, and H. A. Gasteiger, *J. Electrochem. Soc.*, **164**, A2716 (2017).
7. J. Landesfeind, A. Ehrl, M. Graf, W. A. Wall, and H. A. Gasteiger, *J. Electrochem. Soc.*, **163**, A1254 (2016).
8. L. O. Valøen and J. N. Reimers, *J. Electrochem. Soc.*, **152**, A882 (2005).
9. H. Lundgren, M. Behm, and G. Lindbergh, *J. Electrochem. Soc.*, **162**, 3 (2014).
10. A. Nyman, M. Behm, and G. Lindbergh, *Electrochim. Acta*, **53**, 6356 (2008).
11. C. L. Berhaut, P. Porion, L. Timperman, G. Schmidt, D. Lemordant, and M. Anouti, *Electrochim. Acta*, **180**, 778 (2015).
12. P. Bruce and C. Vincent, *J. Electroanal. Chem.*, **225**, 1 (1987).
13. P. G. Bruce, M. T. Hardgrave, and C. A. Vincent, *Solid State Ionics*, **53–56**, 1087 (1992).
14. K. L. Gering, *Electrochim. Acta*, **225**, 175 (2017).
15. K. L. Gering, L. L. Lee, L. H. Landis, and J. L. Savidge, *Fluid Phase Equilib.*, **48**, 111 (1989).
16. E. R. Logan, E. M. Tonita, K. L. Gering, and J. R. Dahn, *J. Electrochem. Soc.*, **165**, 3350 (2018).
17. M. Farkhondeh, M. Pritzker, C. Delacourt, S. S. W. Liu, and M. Fowler, *J. Phys. Chem. C*, **121**, 4112 (2017).
18. L. Ma, S. L. Glazier, R. Petibon, J. Xia, J. M. Peters, Q. Liu, J. Allen, R. N. C. Doig, and J. R. Dahn, *J. Electrochem. Soc.*, **164**, 5008 (2017).
19. J. Landesfeind and H. A. Gasteiger, *J. Electrochem. Soc.*, **this issue** (2019).
20. H. Hafezi and J. Newman, *J. Electrochem. Soc.*, **147**, 3036 (2000).
21. Andrzej Lasia, *Electrochemical Impedance Spectroscopy and its Applications*, Springer, (2014).
22. Mathworks, *Matlab Online Ref.*, **R2017b** https://mathworks.com/help/.
23. A. Nyman, M. Behm, and G. Lindbergh, *Electrochim. Acta*, **53**, 6356 (2008).
24. M. R. Wright, *An Introduction to Aqueous Electrolyte Solutions*, John Wiley & Sons, Ltd, Chichester, (2007).
25. C. H. Hamann, A. Hamnett, and W. Vielstich, *Electrochemistry*, Wiley-VCH, Weinheim, (2007).
26. M. Odziemkowski and D. E. Irish, *J. Electrochem. Soc.*, **140**, 1546 (1993).
27. A. Ehrl, *PhD Thesis*, München (2016).
28. A. J. Bard and L. R. Faulkner, *Electrochemical Methods - Fundamentals and Applications*, 2nd ed., John Wiley & Sons, Inc., New York, (2001).
29. Z. Feng, K. Higa, K. S. Han, and V. Srinivasan, *J. Electrochem. Soc.*, **164**, A2434 (2017).
30. K. Xu, *Chem. Rev.*, **104**, 4303 (2004).
31. N. Chapman, O. Borodin, T. Yoon, C. C. Nguyen, and B. L. Lucht, *Phys. Chem. C*, **121**, 2135 (2017).
32. K. Hayamizu, *J. Chem. Eng. Data*, **57**, 2012 (2012).
33. M. S. Ding, K. Xu, and T. R. Jow, **147**, 1688 (2000).
34. Y. Ma, M. Doyle, T. F. Fuller, M. M. Doeff, L. C. Jonghe, and J. Newman, *J. Electrochem. Soc.*, **142**, 1859 (1995).
35. S. A. Krachkovskiy, J. D. Bazak, S. Fraser, I. C. Halalay, and G. R. Goward, **164**, 912 (2017).
36. J. Wandt, P. Jakes, J. Granwehr, R. Eichel, and H. A. Gasteiger, *Mater. Today*, **21**, 231 (2018).
37. V. Zinth, C. Von Lüders, M. Hofmann, J. Hattendorff, I. Buchberger, S. Erhard, J. Rebelo-Kornmeier, A. Jossen, and R. Gilles, *J. Power Sources*, **271**, 152 (2014).
38. T. Waldmann, B.-I. Hogg, and M. Wohlfahrt-Mehrens, *J. Power Sources*, **384**, 107 (2018).
39. S. Hein and A. Latz, *Electrochim. Acta*, **201**, 354 (2016).
40. O. Borodin, M. Olguin, P. Ganesh, Paul R. C. Kent, Joshua L. Allena, and W. A. Henderson, *Phys. Chem. Chem. Phys.*, **18**, 164 (2016).